Cosmic Ray Studies with The High-Altitude Water Cherenkov Observatory

Wayne Springer
Department of Physics and Astronomy, University of Utah, Salt Lake City, UT, USA
On Behalf of the HAWC Collaboration

- **The HAWC Detector**
  - **Design Principles**
  - **Reconstruction Techniques**
  - **Simulation**
- **HAWC Cosmic Ray Studies**
  - **All-particle Energy Spectrum**
  - **Composition studies**
  - **Anisotropy of Arrival Directions**
  - **Sources of Cosmic Rays – PeVatrons?**
  - **Other cosmic ray-related studies**
- **Summary + Future Outlook**
- **References**

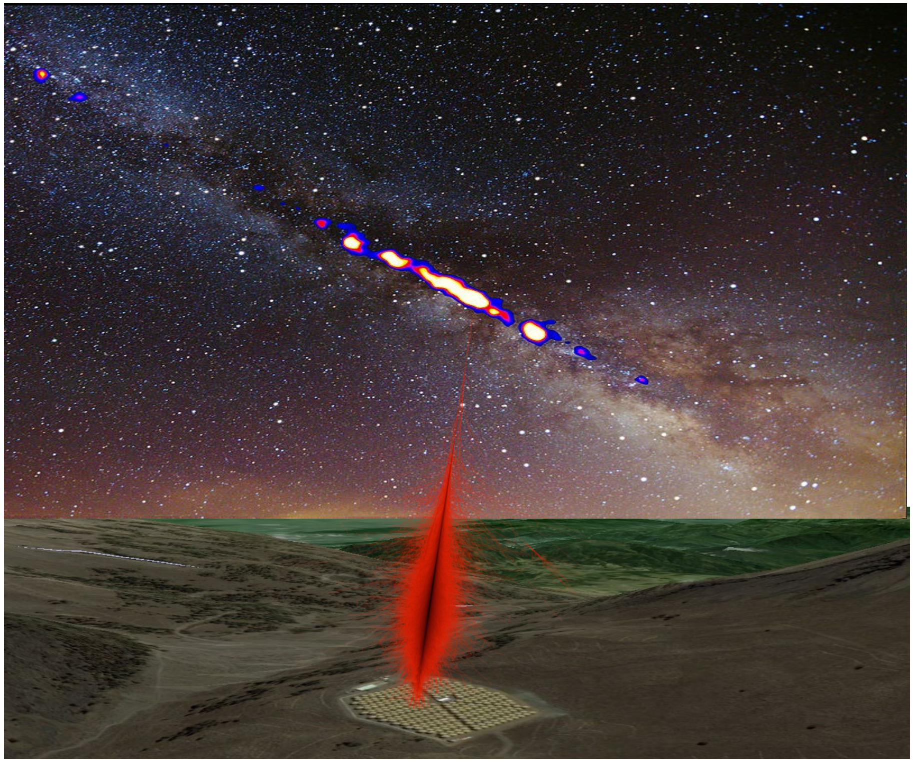

June 17,2024
Trapani,Italy

HAWC Observatory - Design Principles

Atmosphere "converts" particle into an extensive air shower (EAS).

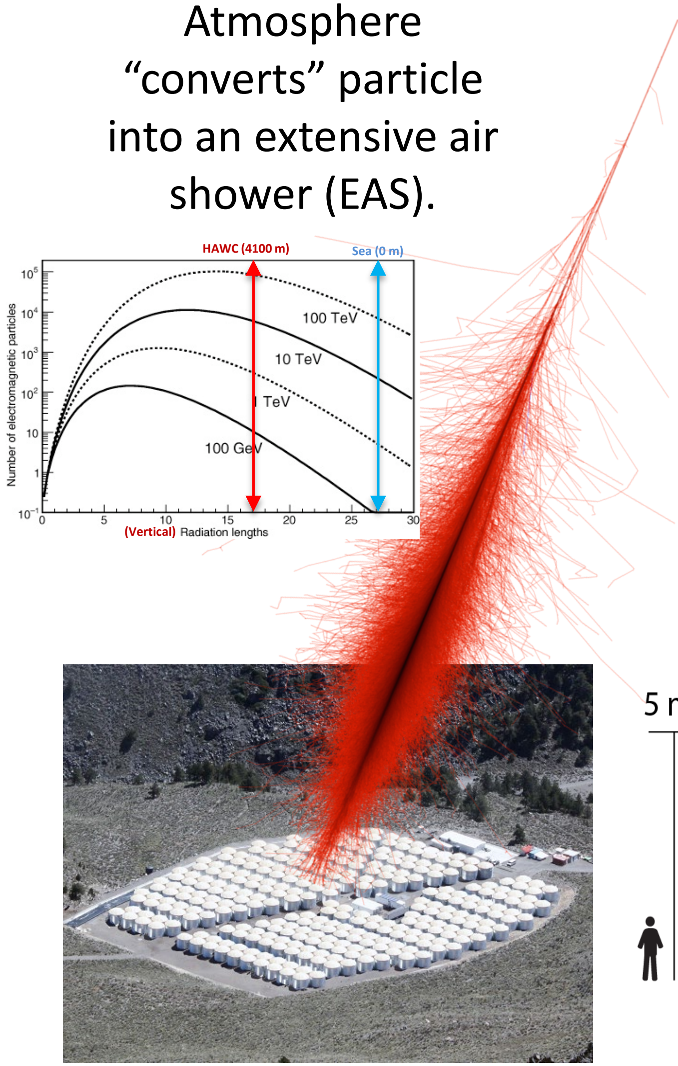

Water Cerenkov Detector Samples Extensive Air Shower particles by measuring their Cerenkov light emitted in water tank.

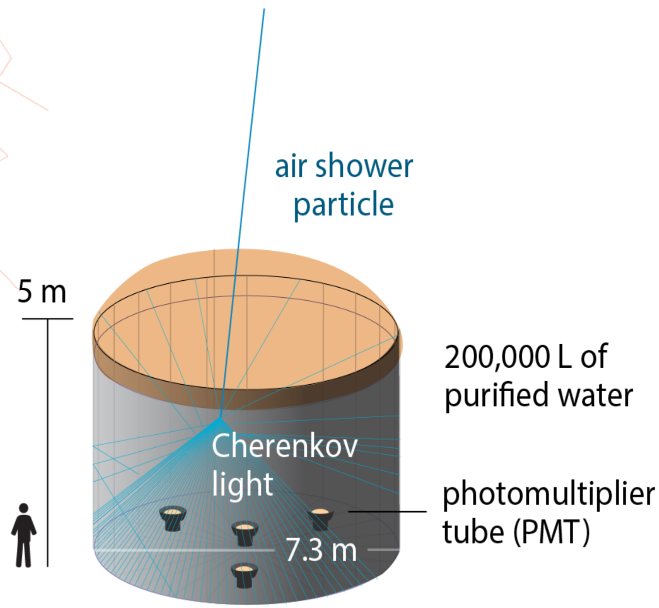

PMT Converts Cerenkov light into electrical signal.

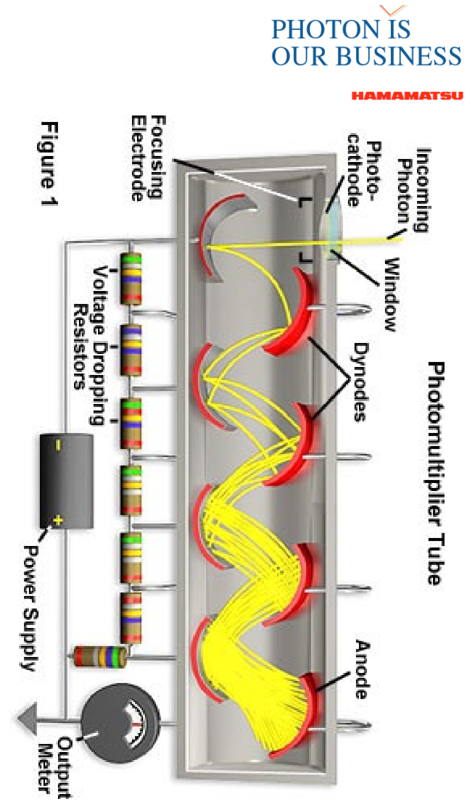

Based upon Milagro Experiment

Reconstruction of Energy & Arrival Direction:

Core Location , Lateral Distribution, Plane Fit

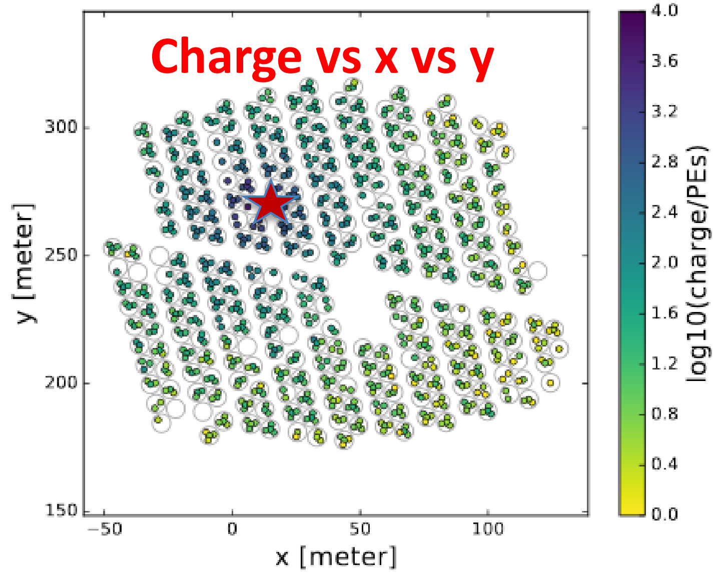

$$x_{COM}, y_{COM} = \frac{\sum_{i=1}^{Nhit} x_i N_{pe,i}}{\sum_{i=1}^{Nhit} N_{pe,i}}, \frac{\sum_{i=1}^{Nhit} y_i N_{pe,i}}{\sum_{i=1}^{Nhit} N_{pe,i}}$$

Location of Maximum Charge Density

Core Location

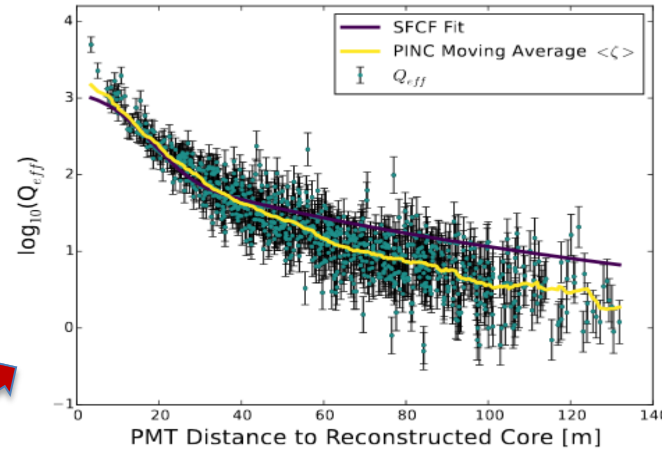

Lateral Distribution Function

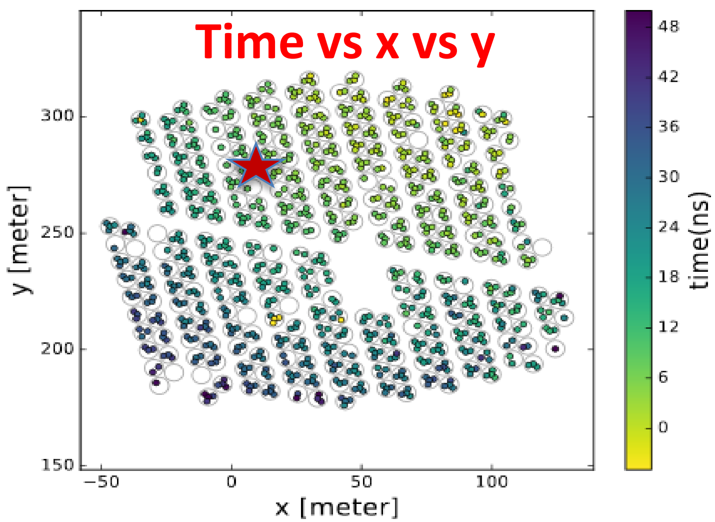

Shower Plane

Zenith θ

Azimuth ϕ

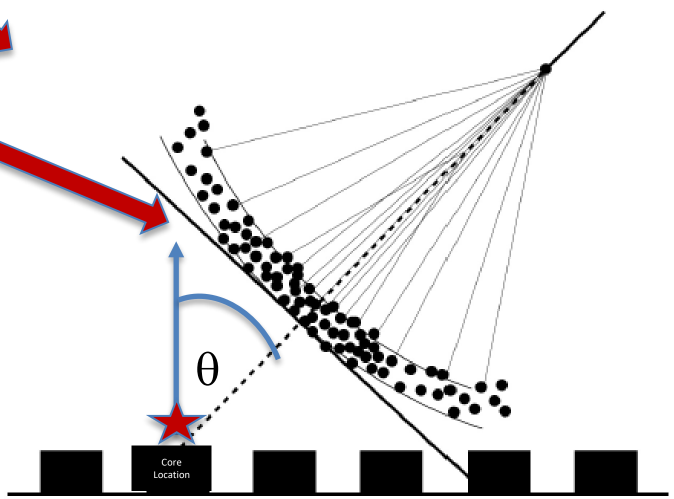

EAS - Energy Reconstruction

Energy Estimator for Cosmic Ray Energy Spectrum Analyses

- "Ground Parameter" from Lateral Distribution function
- Use simulated four-dimensional probability table with bins in: Primary Energy, Zenith angle, PMT distance from core (lateral distance), PMT signal amplitude.
- Perform likelihood fit to PMT signals to obtain energy estimate

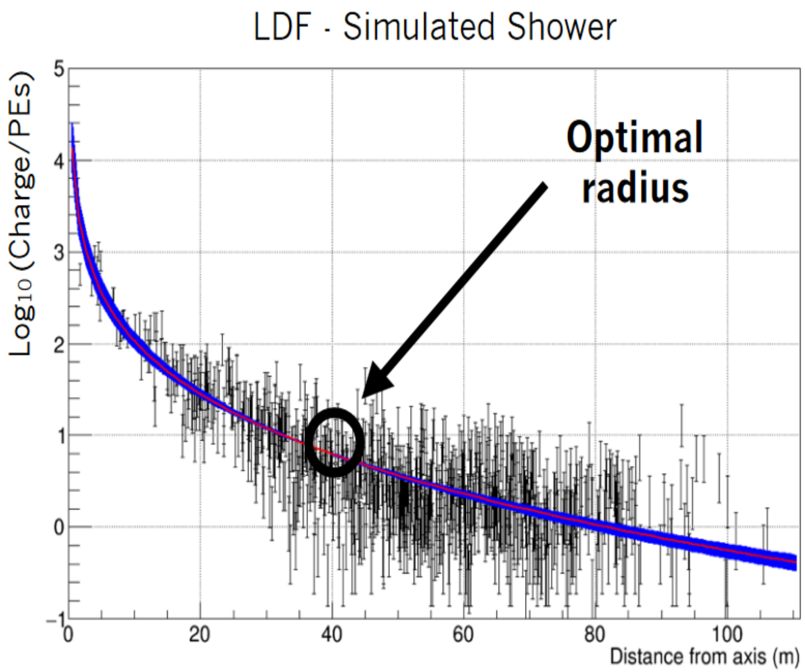

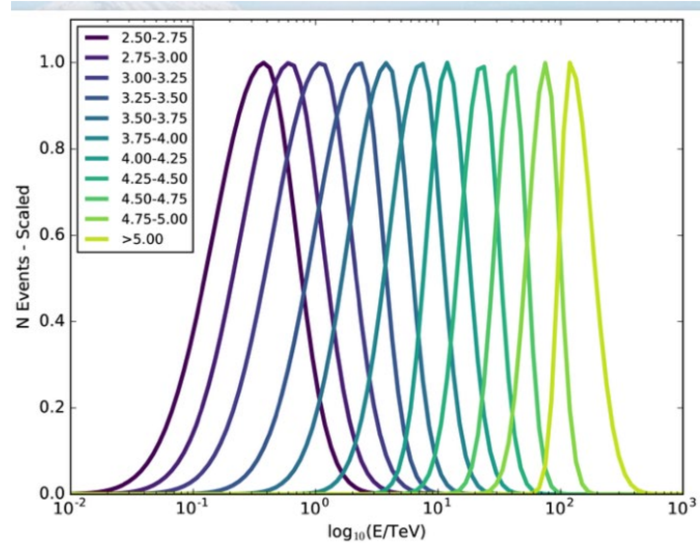

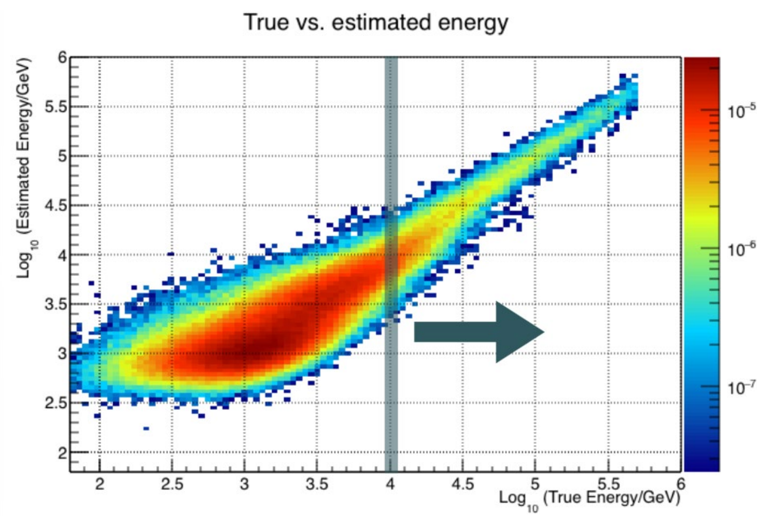

Energy Calibration using The Moon!

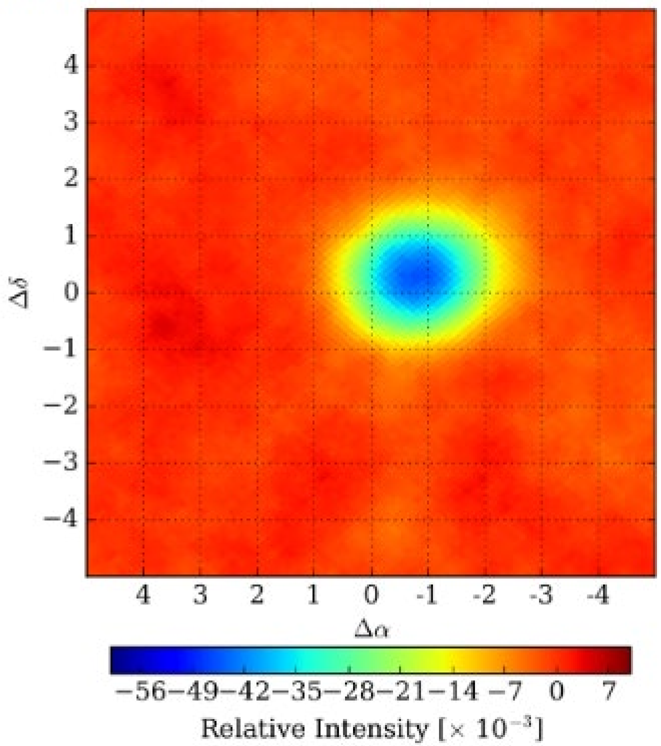

FIG. 5. Relative intensity of the Moon shadow at a mean energy of 4.3 TeV. The map has been smoothed with a top-hat function by 1° to enhance the shadow visually. A two-dimensional Gaussian was fit to the unsmoothed maps.

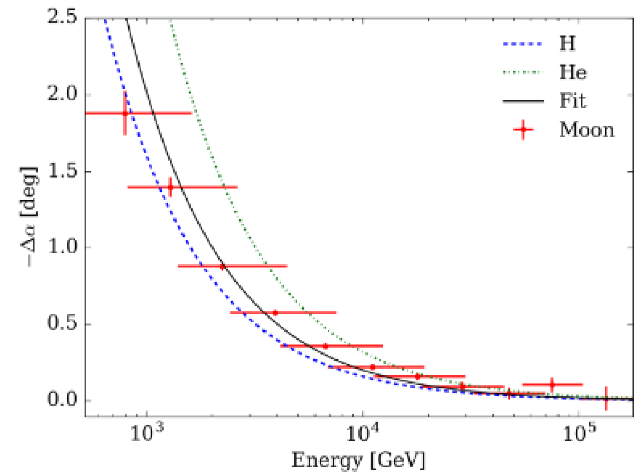

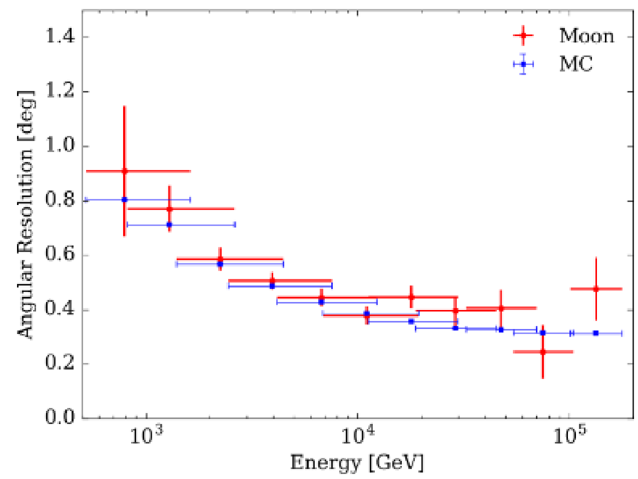

Extensive Air Shower & Detector Simulation

- ❑ Corsika v7.40
  - ❑ Fluka
  - ❑ QGSJet-II-03(04) and EPOS
- ❑ Various Composition Mixes
  - ❑ AMS-2
  - ❑ Cream I-II
  - ❑ PAMELA
  - ❑ ATIC, JACEE,MUBEE
- ❑ Detector Response Software
  - ❑ Based on Geant4

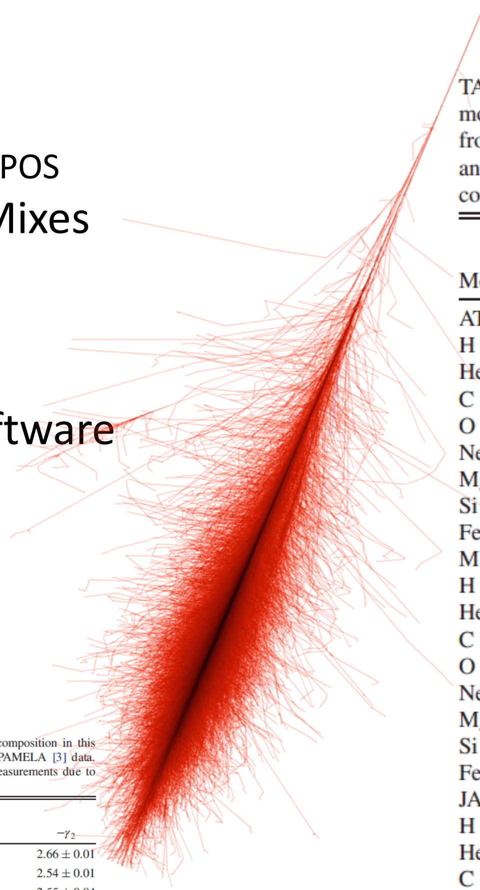

TABLE I. Equation (1) parameters for the hadronic species considered for the assumed composition in this analysis. The parameters were obtained as best fits to AMS [22,23], CREAM [4,6], and PAMELA [3] data. Uncertainties in the fits were included in estimating the systematic uncertainties of flux measurements due to composition assumptions.

	A $[\mathrm{GeV\,s\,sr\,m^2}]^{-1}$	E_{br} [GeV]	$-\gamma_1$	$-\gamma_2$
H	$(4.48 \pm 0.04) \times 10^{-2}$	$440.6^{+87.8}_{-62.7}$	2.81 ± 0.01	2.66 ± 0.01
He	$(3.31 \pm 0.02) \times 10^{-2}$	$854.8^{+125.7}_{-105.5}$	2.73 ± 0.01	2.54 ± 0.01
C	$(6.96 \pm 0.18) \times 10^{-6}$	$2882^{+904.4}_{-481.9}$	2.76 ± 0.03	2.55 ± 0.04
O	$(5.00 \pm 0.09) \times 10^{-6}$	3843^{+1206}_{-643}	2.76 ± 0.03	2.55 ± 0.04
Ne	$(6.31 \pm 0.35) \times 10^{-7}$	4803^{+1507}_{-803}	2.76 ± 0.03	2.55 ± 0.04
Mg	$(5.70 \pm 0.26) \times 10^{-7}$	5764^{+1809}_{-964}	2.76 ± 0.03	2.55 ± 0.04
Si	$(5.70 \pm 0.13) \times 10^{-7}$	6725^{+2110}_{-1124}	2.76 ± 0.03	2.55 ± 0.04
Fe	$(2.00 \pm 0.04) \times 10^{-7}$	13450^{+4220}_{-2249}	2.76 ± 0.03	2.55 ± 0.04

https://journals.aps.org/prd/pdf/10.1103/PhysRevD.96.122001

TABLE III. Values of the parameters of three composition models used in the present analysis. The models were derived from fits with expression (A1) to the ATIC-2 [90], JACEE [65], and MUBEE [91] measurements on the elemental spectra of cosmic rays.

Model	Φ_0 $[10^{-6}\,\mathrm{m^{-2}\,s^{-1}\,sr^{-1}\,GeV^{-1}}]$	γ_1	γ_2	E_b [GeV]
ATIC-2				
H	4.40×10^4	−2.86	−2.60	159.6
He	2.59×10^4	−2.61	−2.45	1093.6
C	6.61	−2.64	−2.48	11125.5
O	10.73	−2.64	−2.48	11125.5
Ne	2.78	−2.64	−2.48	11125.5
Mg	4.72	−2.64	−2.48	11125.5
Si	5.34	−2.64	−2.48	11125.5
Fe	13.10	−2.61	−2.48	11125.5
MUBEE				
H	4.44×10^4	−2.72	−2.72	–
He	2.66×10^4	−2.60	−2.63	732.7
C	6.41	−2.64	−2.56	31693.5
O	10.46	−2.64	−2.56	31693.5
Ne	2.46	−2.64	−2.00	31693.5
Mg	4.13	−2.64	−2.00	31693.5
Si	4.58	−2.64	−2.00	31693.5
Fe	13.10	−2.61	−3.00	4283.8
JACEE				
H	4.39×10^4	−2.80	−2.69	109.44
He	2.67×10^4	−2.60	−2.59	1586.4
C	6.35	−2.64	−2.24	13106.9
O	10.35	−2.64	−2.24	13106.9
Ne	2.46	−2.64	−2.48	31693.5
Mg	4.13	−2.64	−2.48	31693.5
Si	4.58	−2.64	−2.48	31693.5
Fe	13.10	−2.61	−2.51	80717.9

https://journals.aps.org/prd/pdf/10.1103/PhysRevD.105.063021

Cosmic Ray Studies – All-particle Energy Spectrum

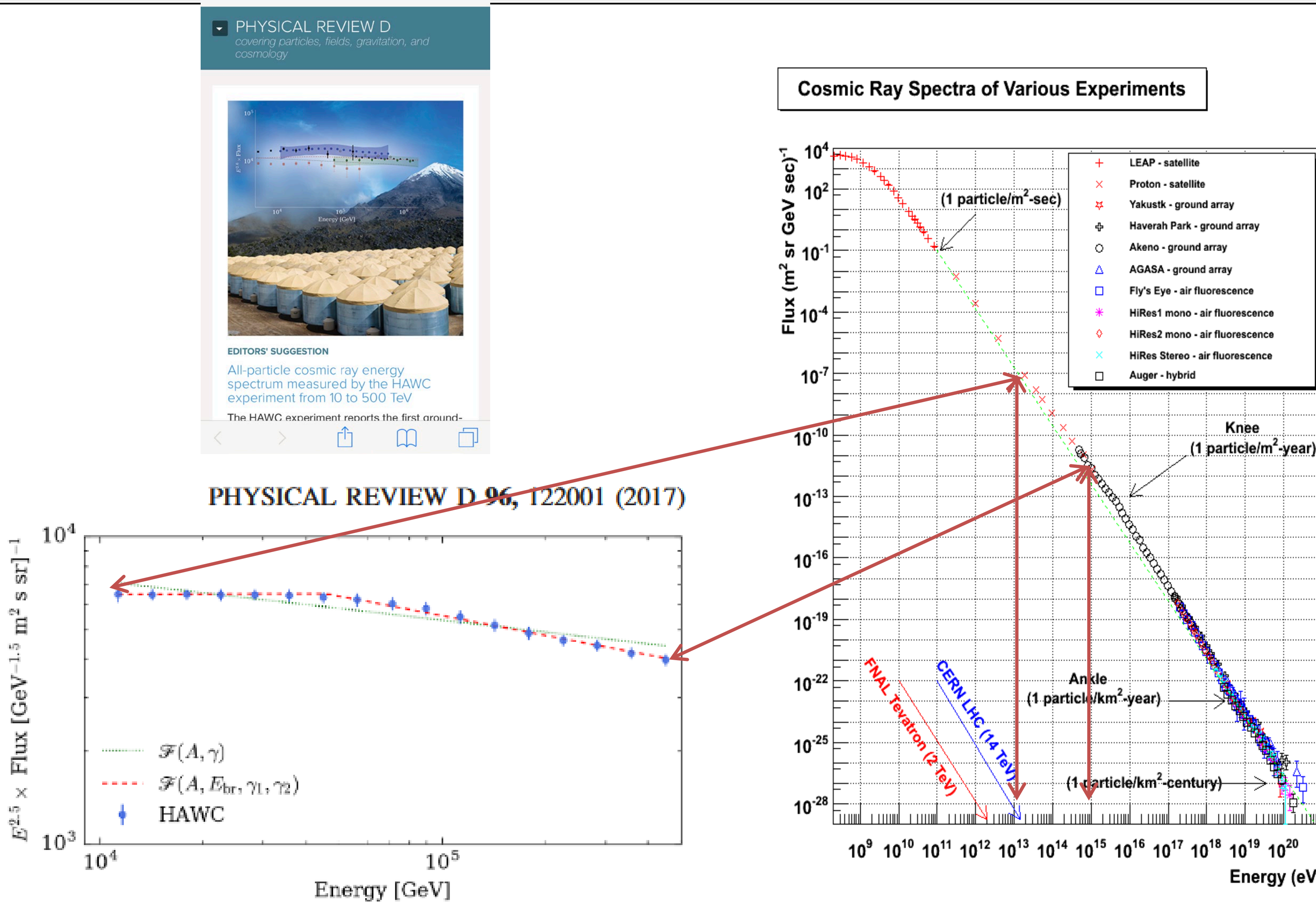

https://journals.aps.org/prd/abstract/10.1103/PhysRevD.96.122001

Where do high-energy cosmic ray originate?

All-particle Energy Spectrum Analysis

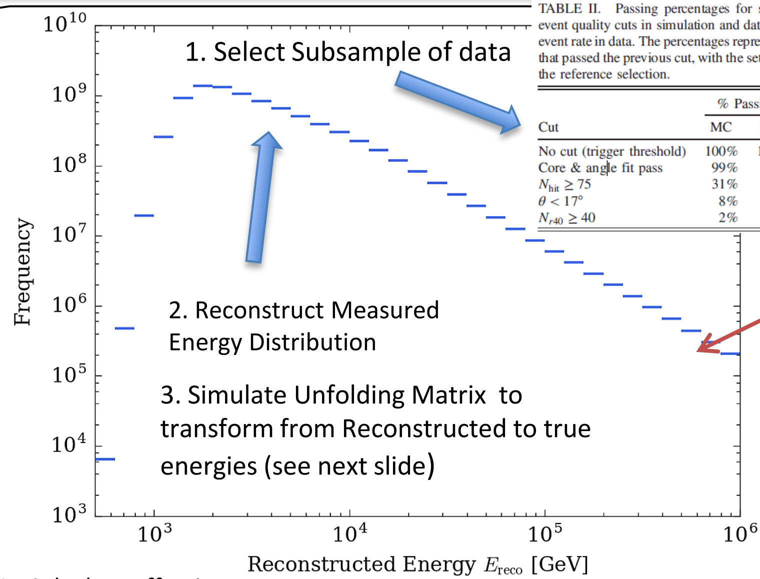

TABLE II. Passing percentages for successive application of event quality cuts in simulation and data, including the observed event rate in data. The percentages represent the fraction of events that passed the previous cut, with the set of triggered events being the reference selection.

	% Passing		Data Event Rate
Cut	MC	Data	[kHz]
No cut (trigger threshold)	100%	100%	24.7
Core & angle fit pass	99%	96%	23.6
$N_{hit} \geq 75$	31%	23%	5.7
$\theta < 17°$	8%	6%	1.5
$N_{r40} \geq 40$	2%	2%	0.43

Flux Formula:

$$\Phi(E) = \frac{N(E)}{\Delta E \Delta t A_{eff}(E) \Delta \Omega}$$

- Φ(E): Energy Spectrum: Intensity as a function of Energy
- N(E): Number of selected events in energy bin with mean energy E. Sum= 7.2x10^{10} EAS events
- ΔE: width of energy bin with mean energy E
- Δt: exposure time = 5.3 years
- $\Delta\Omega$: solid angle = 1.14 sr
- A_{eff}(E): Effective Area as a function of Energy

4. Calculate effective area

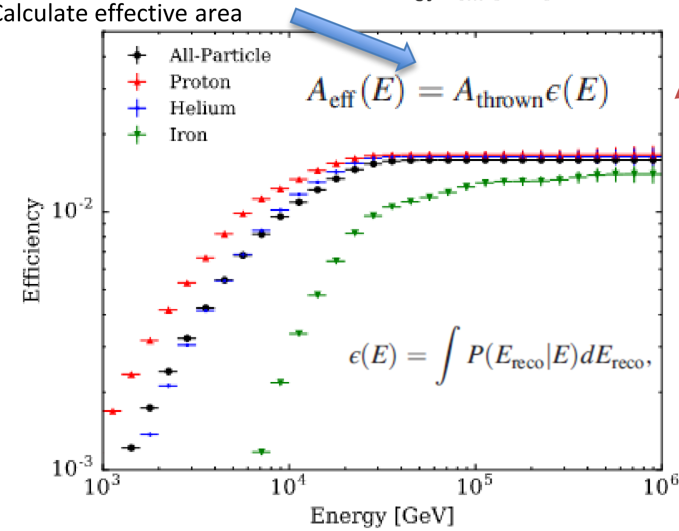

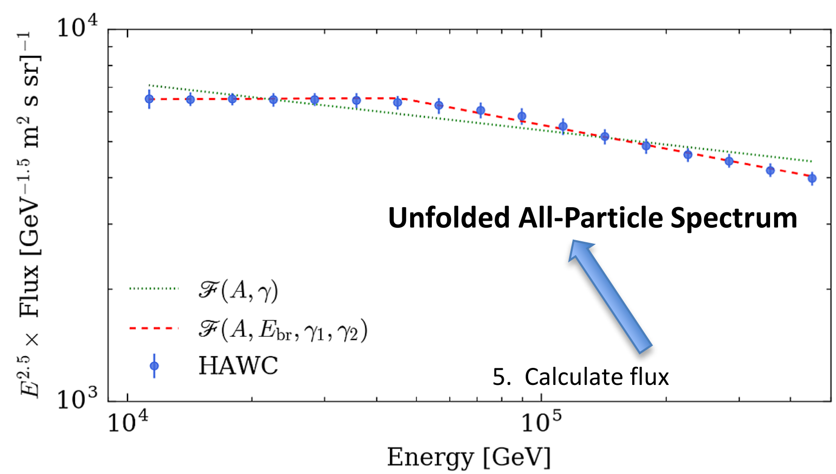

All-particle Energy Spectrum Analysis:
Composition Dependence & Energy Unfolding

Unfolding to transform from Reconstructed to true energies

$$P(E|E_{\text{reco}}) = \frac{P(E_{\text{reco}}|E)P(E)}{\epsilon(E)\sum_{E'}P(E_{\text{reco}}|E')P(E')},$$

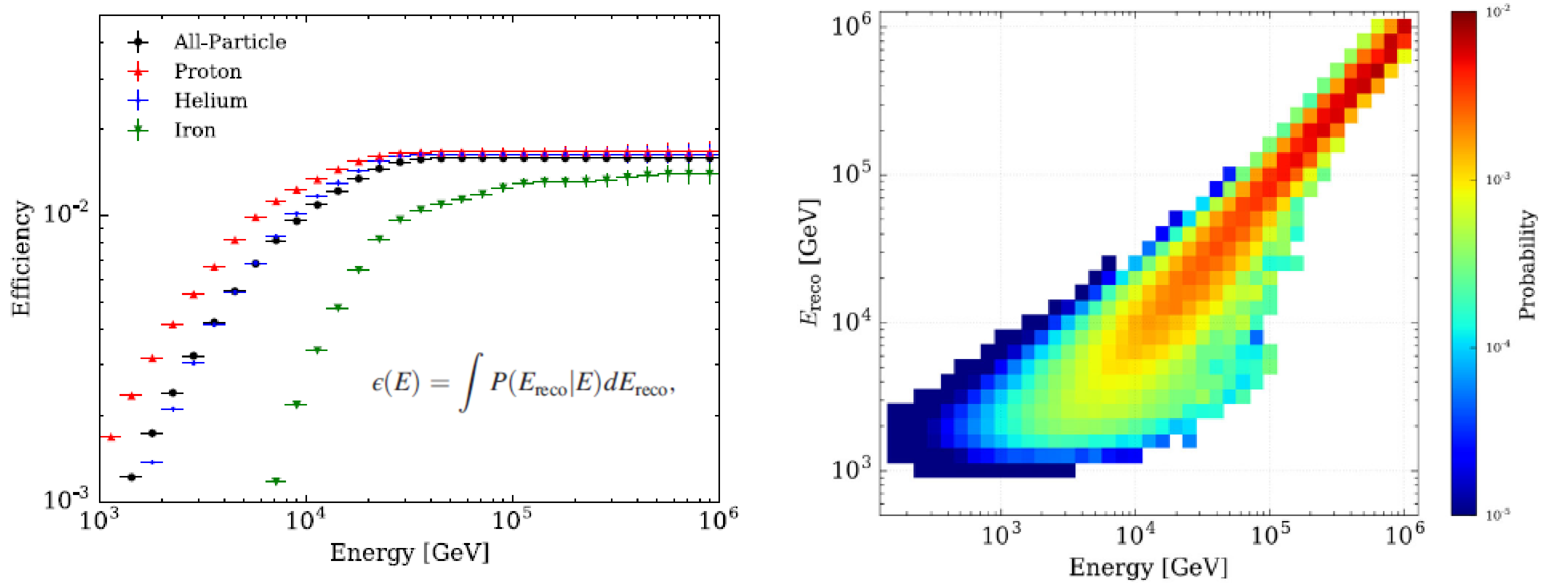

FIG. 7. The left panel shows the efficiencies $\epsilon(E)$ for all combined cosmic ray particles and individually for proton, helium, and iron components. The energy response matrix $P(E_{\text{reco}}|E)$ for all species using the composition defined in Table I is shown on the right. The deviation from the diagonal and the width of $P(E_{\text{reco}}|E)$ are simply the bias and resolution, respectively, already presented in Fig. 4.

$$N(E) = \sum_{E_{\text{reco}}} N(E_{\text{reco}})P(E|E_{\text{reco}}).$$

$$A_{\text{eff}}(E) = A_{\text{thrown}}\epsilon(E)$$

$$\Phi(E) = \frac{N(E)}{\Delta E \Delta t A_{eff}(E)\Delta\Omega}$$

All-particle Energy Spectrum Analysis:

Results, Systematic Uncertainties & Comparisons

TABLE IV. Values of the all-particle cosmic-ray energy spectrum from 10–500 TeV including uncertainties. The second column is the number of events unfolded, or the distribution $N(E)$. The label "stat" represents the statistical uncertainties, "sys_{MC}" is for the uncertainties from the limited amount of simulation, and "sys" represents the remaining sources of systematic uncertainty added in quadrature.

$\log E/\mathrm{GeV}$	N_{events} Unfolded	$\frac{dN}{dE d\Omega dt dA} \pm \mathrm{stat} \pm \mathrm{sys_{MC}} + \mathrm{sys} - \mathrm{sys} [\mathrm{GeV\ s\ m^2\ sr}]^{-1}$
4.0–4.1	2.00×10^{10}	$(4.7968 \pm 0.0002 \pm 0.5901 + 0.4288 - 0.8530) \times 10^{-7}$
4.1–4.2	1.42×10^{10}	$(2.6922 \pm 0.0001 \pm 0.2323 + 0.2360 - 0.4467) \times 10^{-7}$
4.2–4.3	1.00×10^{10}	$(1.5163 \pm 0.0001 \pm 0.1189 + 0.1315 - 0.2356) \times 10^{-7}$
4.3–4.4	7.08×10^{9}	$(8.4947 \pm 0.0007 \pm 0.7137 + 0.7352 - 1.2419) \times 10^{-8}$
4.4–4.5	5.02×10^{9}	$(4.7823 \pm 0.0005 \pm 0.3896 + 0.4171 - 0.6614) \times 10^{-8}$
4.5–4.6	3.54×10^{9}	$(2.6761 \pm 0.0003 \pm 0.2536 + 0.2377 - 0.3522) \times 10^{-8}$
4.6–4.7	2.47×10^{9}	$(1.4823 \pm 0.0002 \pm 0.1305 + 0.1357 - 0.1869) \times 10^{-8}$
4.7–4.8	1.71×10^{9}	$(8.1839 \pm 0.0015 \pm 0.8041 + 0.7830 - 0.9947) \times 10^{-9}$
4.8–4.9	1.18×10^{9}	$(4.4769 \pm 0.0010 \pm 0.4488 + 0.4547 - 0.5281) \times 10^{-9}$
4.9–5.0	8.03×10^{8}	$(2.4193 \pm 0.0007 \pm 0.2504 + 0.2655 - 0.2787) \times 10^{-9}$
5.0–5.1	5.34×10^{8}	$(1.2781 \pm 0.0004 \pm 0.1349 + 0.1544 - 0.1447) \times 10^{-9}$
5.1–5.2	3.56×10^{8}	$(6.7636 \pm 0.0027 \pm 0.6441 + 0.9164 - 0.7576) \times 10^{-10}$
5.2–5.3	2.37×10^{8}	$(3.5835 \pm 0.0017 \pm 0.3331 + 0.5544 - 0.3995) \times 10^{-10}$
5.3–5.4	1.59×10^{8}	$(1.9107 \pm 0.0011 \pm 0.1644 + 0.3430 - 0.2134) \times 10^{-10}$
5.4–5.5	1.09×10^{8}	$(1.0346 \pm 0.0007 \pm 0.0892 + 0.2184 - 0.1166) \times 10^{-10}$
5.5–5.6	7.25×10^{7}	$(5.4882 \pm 0.0047 \pm 0.4659 + 1.3920 - 0.6286) \times 10^{-11}$
5.6–5.7	4.87×10^{7}	$(2.9284 \pm 0.0030 \pm 0.2402 + 0.9642 - 0.3441) \times 10^{-11}$

TABLE III. Summary of systematic uncertainties. The contribution from each source was determined by varying that source independently, while holding all others fixed at their nominal values. The contributions from all sources are added in quadrature to conservatively estimate the total systematic uncertainty.

	10 TeV	100 TeV	1 PeV
PMT QE	±6%	±8%	±9%
PMT Q_{res}	−3%	−5%	−10%
Simulation	±8%	±8%	±8%
Composition	−16/ + 5%	−4/ + 3%	±3%
Hadronic Int.	+5%	+10%	−4/ + 2%
Total	−20/ + 12%	−14/ + 15%	−20/ + 13%

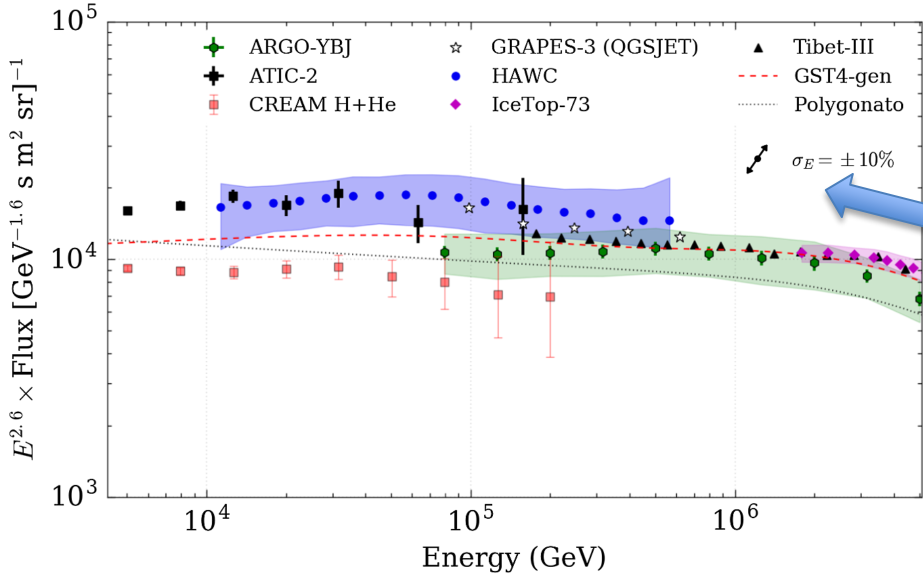

Effect of Energy Scale Uncertainty

Cosmic Ray Spectrum of Protons Plus Helium (PRD2022)

$$\Phi(E) = \frac{N(E)}{\Delta E \Delta t A_{eff}(E) \Delta\Omega}$$

https://journals.aps.org/prd/abstract/10.1103/PhysRevD.105.063021

- $\Phi(E)$: Energy Spectrum: Intensity as a function of Energy
- $N(E)$: Number of selected events in energy bin with mean energy E. Sum = 7.2×10^{10} EAS events
- ΔE: width of energy bin with mean energy E
- Δt: exposure time = 3.74 years
- $\Delta\Omega$: solid angle = 1.14 sr
- $A_{eff}(E)$: Effective Area as a function of Energy

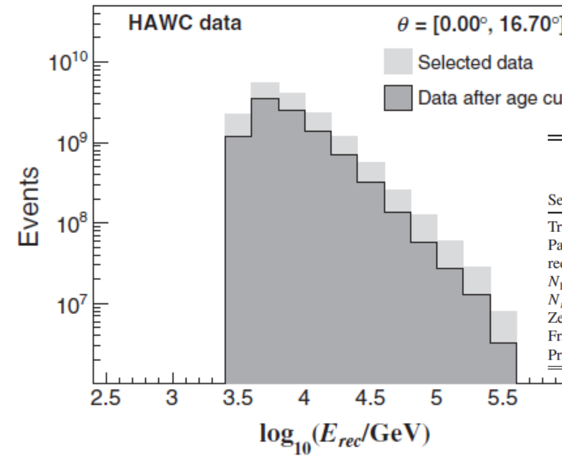

Selection cut	% of remaining events respect to previous cut: Data	MC	Measured rate (kHz)
Trigger	100.00	100.00	24.61
Passed angle and core reconstruction	95.18	100.00	23.42
$N_{hit} \geq 75$	23.65	26.95	5.54
$N_{r40} \geq 40$	26.70	28.39	1.48
Zenith angle	27.82	29.35	0.41
Fraction hit	36.02	31.11	0.15
Primary energy	93.48	92.94	0.14

Cosmic ray spectrum of protons plus helium nuclei between 6 and 158 TeV from HAWC data

A. Albert *et al.*
Phys. Rev. D **105**, 063021 – Published 25 March 2022

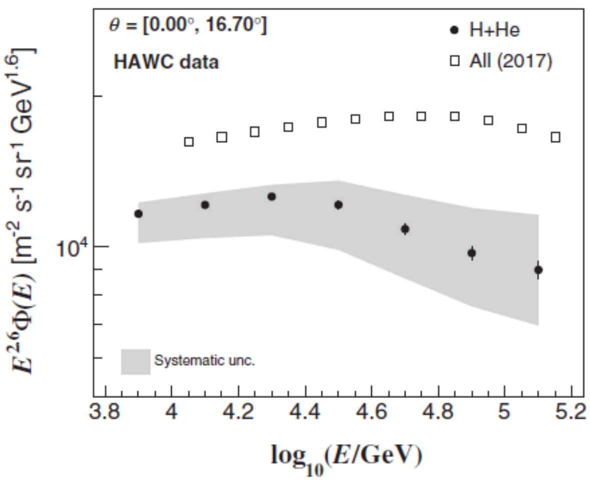

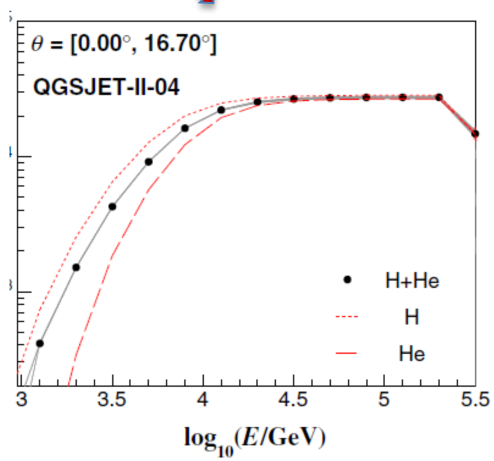

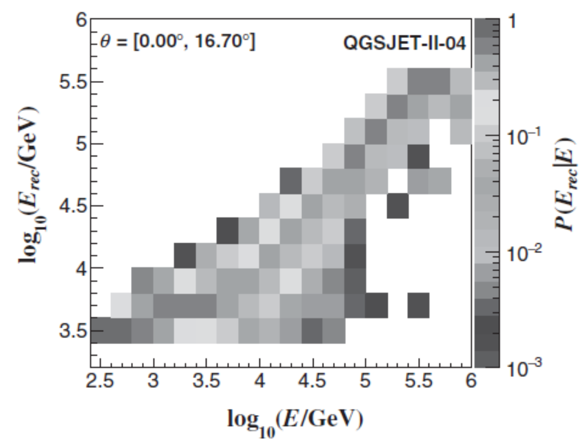

In HAWC, the lateral age of EAS is obtained event by event from a χ^2 fit with a modified Nishimura-Kamata-Greisen function,

$$f(r) = A\left(\frac{r}{r_0}\right)^{s-3}\left(1+\frac{r}{r_0}\right)^{s-4.5}, \qquad (1)$$

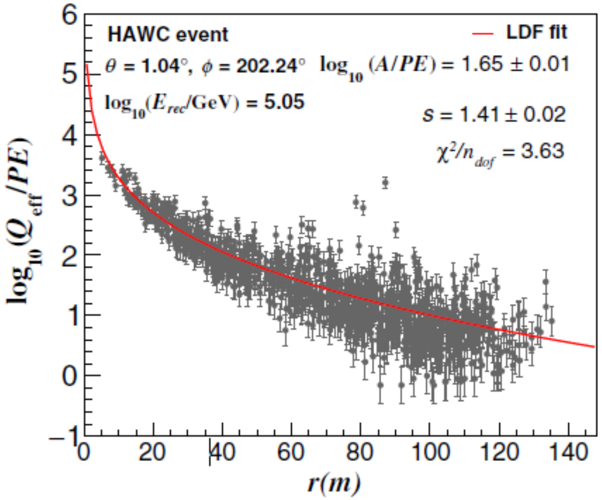

FIG. 1. The lateral effective charge distribution of an EAS event measured with HAWC on June 2, 2019. The estimated energy, zenith angle, and azimuth are $\log_{10}(E_{rec}/\mathrm{GeV}) = 5.05$, $\theta = 1.04°$, and $\phi = 202.24°$, respectively. The gray dots represent the measured Q_{eff} per PMT in PE (photoelectron) units. The vertical errors are the systematic uncertainties. The result of the fit with Eq. (1) is shown with a red line. The corresponding fit parameters are shown; the number of degrees of freedom is 1018.

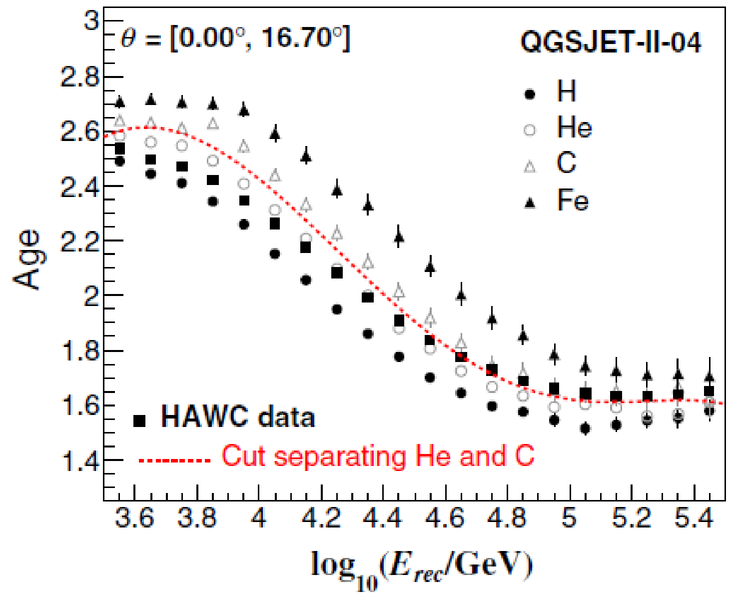

FIG. 4. Predictions of the QGSJET-II-04 model for the energy dependence of the mean lateral age in vertical air showers initiated by four cosmic ray species at HAWC. From top to bottom, the MC points correspond to Fe (solid triangles), C (hollowed triangles), He (hollowed circles), and H (solid circles) primaries, respectively. For clarity, not all the elemental nuclei simulated in this work were included in the plot. HAWC data has also been added to the figure. They are shown with black squares. The $s_{\mathrm{He-C}}$ cut employed to extract the enriched subsample of light nuclei is plotted using a dashed line in red.

Cosmic Ray Spectrum of Protons Plus Helium: Results & comparison

- Energy Unfolding & Age-dependent cuts have enabled the measurement of the composition dependence of the Energy Spectrum of Cosmic Rays
- Results for the proton plus helium component are presented here from the referenced paper.
- Further development work on Energy Estimators using Neural Networks
- Work is ongoing to further decompose energy spectrum into proton, helium and heavy mass groups of cosmic rays (https://pos.sissa.it/444/299/pdf)

E [GeV]	$\Phi(E) \pm \delta\Phi_{stat} + \delta\Phi_{syst} - \delta\Phi_{syst}$ [$m^{-2}s^{-1}$ sr^{-1} GeV^{-1}]
7.94×10^3	$(8.44 \pm 0.07 + 0.45 - 1.06) \times 10^{-7}$
1.26×10^4	$(2.66 \pm 0.03 + 0.14 - 0.38) \times 10^{-7}$
2.00×10^4	$(8.34 \pm 0.12 + 0.46 - 1.36) \times 10^{-8}$
3.16×10^4	$(2.42 \pm 0.05 + 0.29 - 0.45) \times 10^{-8}$
5.01×10^4	$(6.55 \pm 0.16 + 1.11 - 1.33) \times 10^{-9}$
7.94×10^4	$(1.77 \pm 0.05 + 0.41 - 0.39) \times 10^{-9}$
1.26×10^5	$(4.95 \pm 0.19 + 1.43 - 1.12) \times 10^{-10}$

$$\Phi(E) = \Phi_0 E^{\gamma_1},$$

$$\Phi_0 = 10^{4.32\pm0.02}\ m^{-2}\ s^{-1}\ sr^{-1}\ GeV^{-1},$$

$$\gamma_1 = -2.66 \pm 0.01,$$

$$\chi_0^2 = 177.51, \text{ for } \nu_0 = 5 \text{ degrees of freedom}$$

$$\Phi(E) = \Phi_0 E^{\gamma_1}\left[1 + \left(\frac{E}{E_0}\right)^{\epsilon}\right]^{(\gamma_2-\gamma_1)/\epsilon},$$

$$\Phi_0 = 10^{3.71\pm0.09}\ m^{-2}\ s^{-1}\ sr^{-1}\ GeV^{-1},$$

$$\gamma_1 = -2.51 \pm 0.02,$$

$$\gamma_2 = -2.83 \pm 0.02,$$

$$E_0 = 10^{4.38\pm0.06}\ GeV,$$

$$\epsilon = 9.8 \pm 4.1.$$

$\chi_1^2 = 0.26$ For 2 degrees of freedom

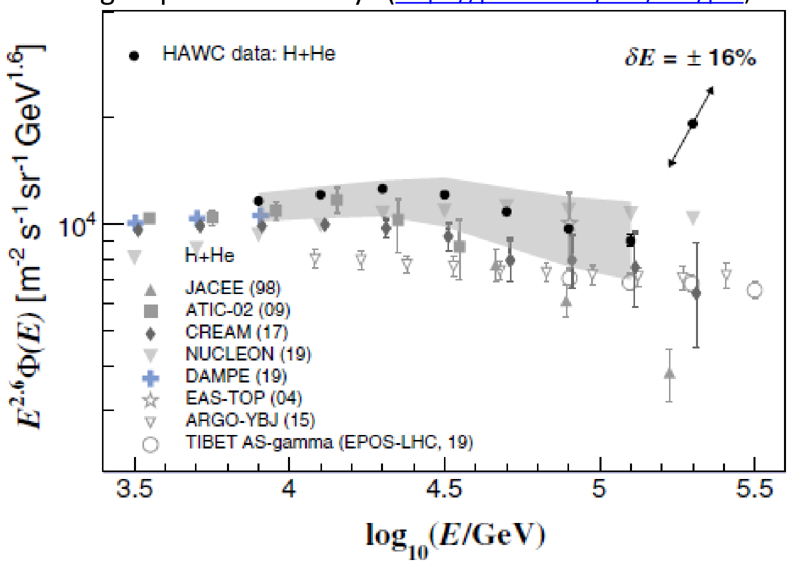

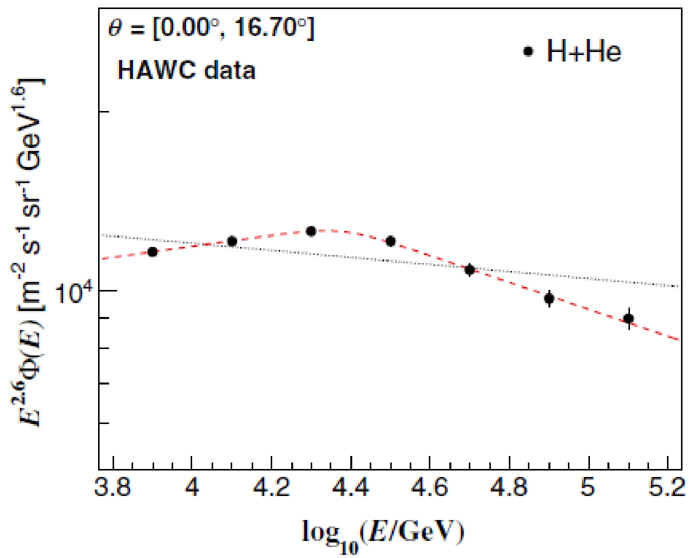

Observation of Anisotropy of TeV Cosmic Rays with Two Years of HAWC

https://doi.org/10.3847/1538-4357/aad90c

- ❑ Anisotropy at all angular scales as a function of energy examined using 1.2 x 10^{12} events over 508 uninterrupted sidereal days measured with 294 WCDs.
- ❑ Varying detector exposure accounted for using an iterative maximum-likelihood fitting technique.
- ❑ Large-scale anisotropy evaluated using multipole fits to arrival direction maps.
- ❑ Small-scale anisotropy evaluated by subtracting Large-scale anisotropy (multipole fit for $l \leq 3$)

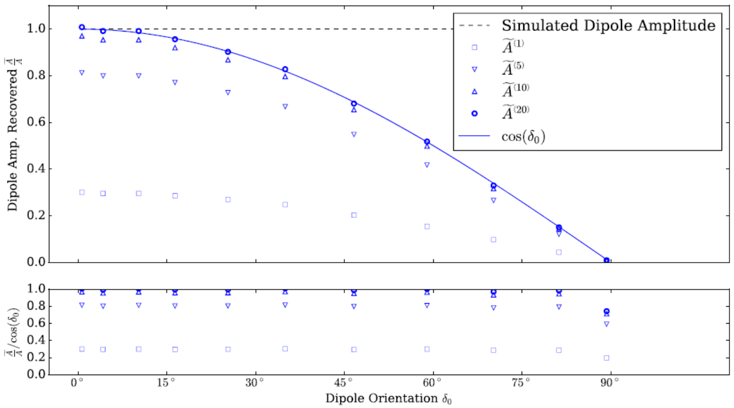

Table 1
Reported Median Energy (With 68% Central Containment Region) and Fit of Two-dimensional Dipole Anisotropy (Amplitude and Phase) for Each Independent Energy Bin

Energy (TeV)	Events	Amplitude [$\times10^{-4}$]	Phase	$a_{1,1}$ [$\times10^{-4}$]	$a_{1,-1}$ [$\times10^{-4}$]	χ^2/N_{dof}
$2.0(^{-1.4}_{+5.2})$	4.0×10^{10}	8.1 ± 0.4	$42.9° \pm 2.5°$	-17.1 ± 1.0	-15.9 ± 1.0	13.34
$3.0(^{-2.1}_{+7.1})$	2.9×10^{10}	8.9 ± 0.3	$52.2° \pm 2.0°$	-15.9 ± 0.9	-20.5 ± 0.9	1.24
$4.4(^{-3.2}_{+10.6})$	2.4×10^{10}	8.3 ± 0.3	$45.6° \pm 1.8°$	-16.7 ± 0.7	-17.1 ± 0.7	0.79
$6.8(^{-5.0}_{+14.0})$	1.6×10^{10}	10.1 ± 0.3	$39.5° \pm 1.6°$	-22.7 ± 0.8	-18.7 ± 0.8	0.85
$11.2(^{-7.9}_{+18.8})$	7.9×10^{9}	11.9 ± 0.4	$41.3° \pm 1.9°$	-25.9 ± 1.1	-22.7 ± 1.1	0.81
$18.6(^{-12.7}_{+25.6})$	3.8×10^{9}	13.8 ± 0.6	$44.5° \pm 2.4°$	-28.4 ± 1.6	-27.9 ± 1.6	1.07
$30.3(^{-19.3}_{+34.8})$	1.8×10^{9}	14.4 ± 0.8	$36.0° \pm 3.2°$	-33.7 ± 2.3	-24.5 ± 2.3	1.25
$72.8(^{-44.9}_{+106.7})$	1.6×10^{9}	6.7 ± 0.9	$31.9° \pm 7.3°$	-16.4 ± 2.5	-10.2 ± 2.5	1.03

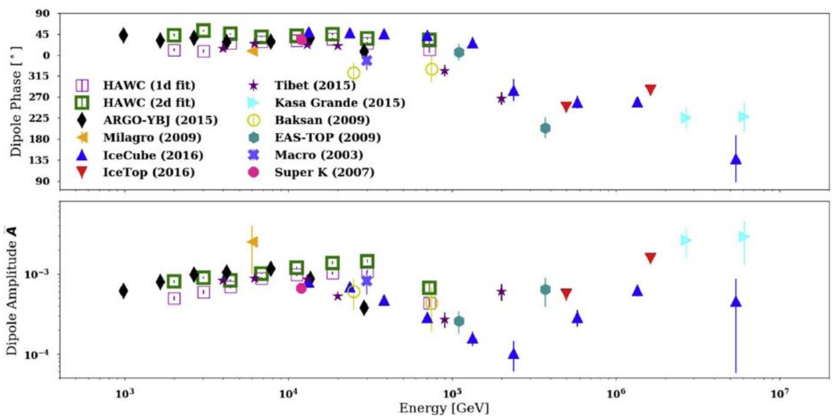

Observation of Anisotropy of TeV Cosmic Rays with Two Years of HAWC

Large-Scale Anisotropy Maps

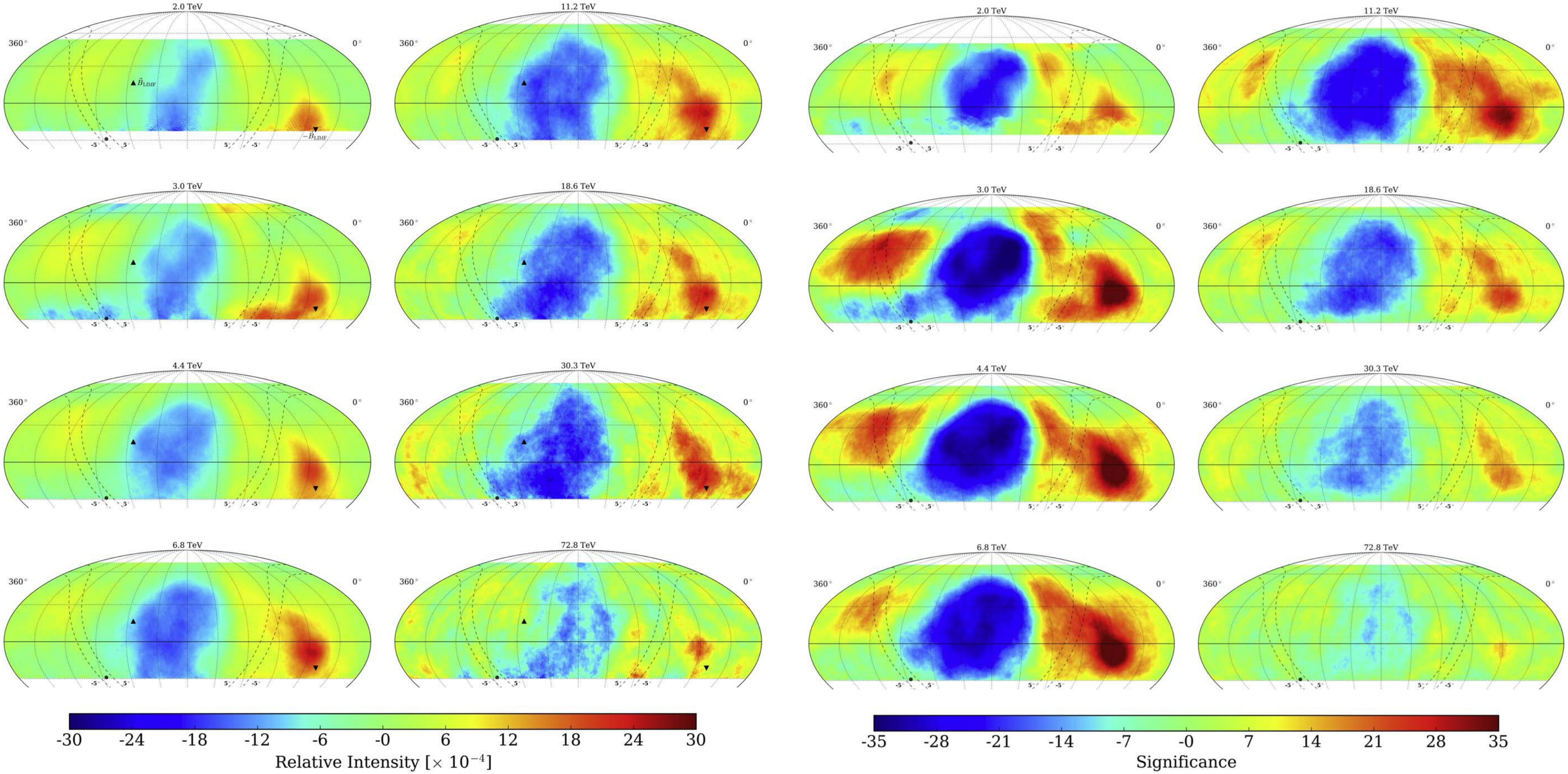

Observation of Anisotropy of TeV Cosmic Rays with Two Years of HAWC

Small-Scale Anisotropy Maps – A multipole fit with l<=3 has been removed

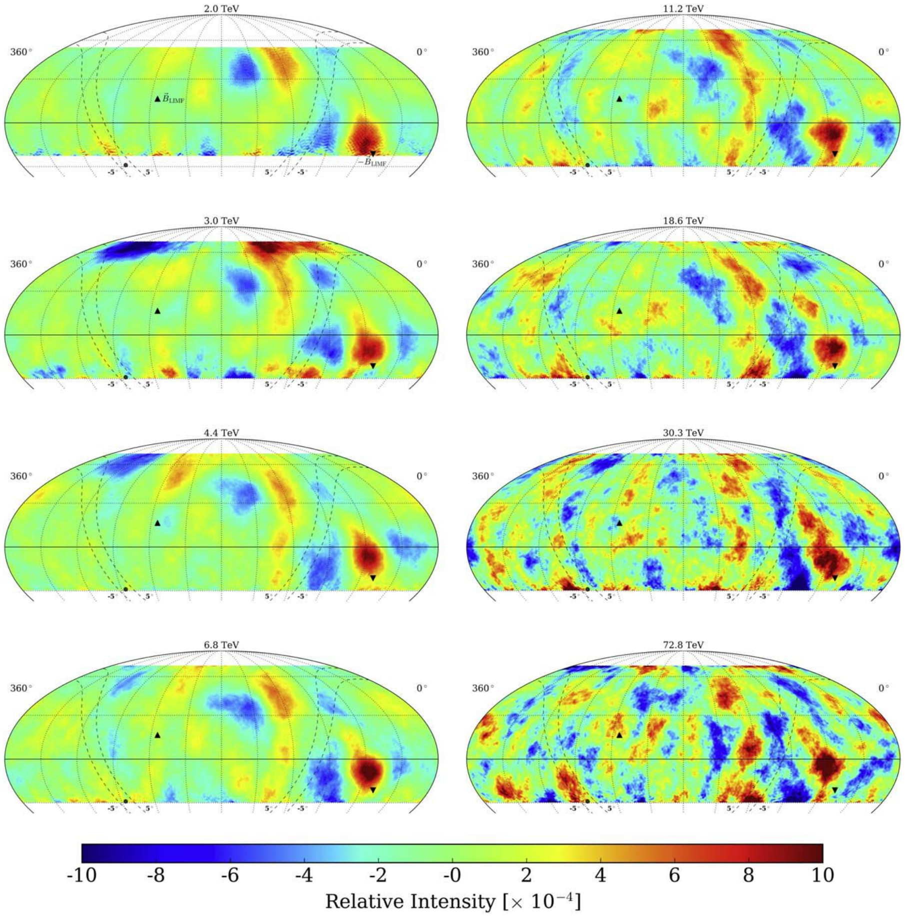

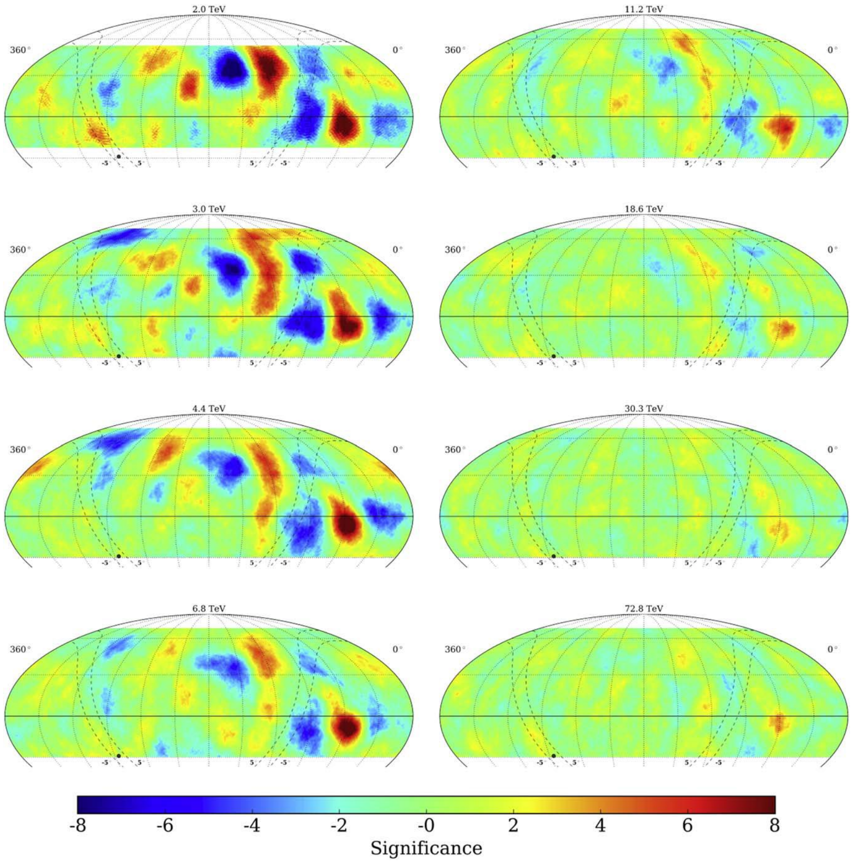

Observation of Anisotropy of TeV Cosmic Rays with Two Years of HAWC

Small-Scale Anisotropy Maps – A multipole fit with l<=3 has been removed

- Significant cosmic-ray anisotropy observed on both large and small angular scales.
- Energy estimation technique with good resolution and energy scale verified by Moon shadow deflection over the range of 2-78 TeV
- Energy dependence of the large-scale phase and amplitude is consistent with other detectors in the northern hemisphere.
- The morphology and relative intensity of the regions exhibiting small-scale regions of excess are also consistent with previous observations.
- The techniques used for this analysis allow for the combination of HAWC data with other experiments such as IceCube….

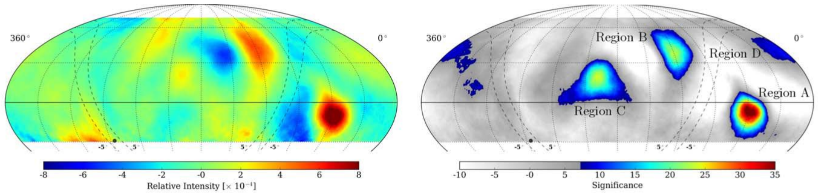

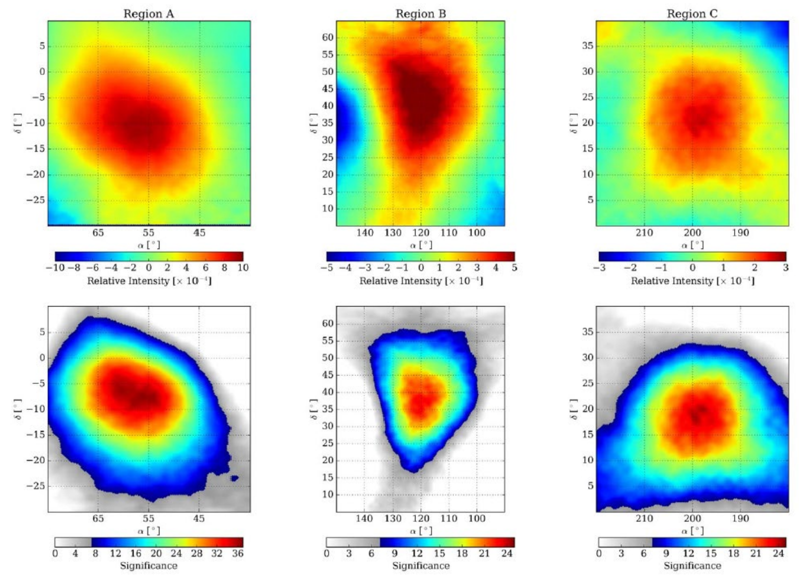

Figure 12. Localized views of the relative intensity (top row) and significance (bottom row) of Regions A (left), B (center), and C (right) having combined all energy bins into a single map. The coordinates of the maximally significant pixels found for each region are presented in Table 2. The scales for the relative intensity and significance are different for each region.

Cosmic Ray Anisotropy – All Sky

The Astrophysical Journal, 871:96 (15pp), 2019 January 20 https://doi.org/10.3847/1538-4357/aaf5cc

CrossMark

All-sky Measurement of the Anisotropy of Cosmic Rays at 10 TeV and Mapping of the Local Interstellar Magnetic Field

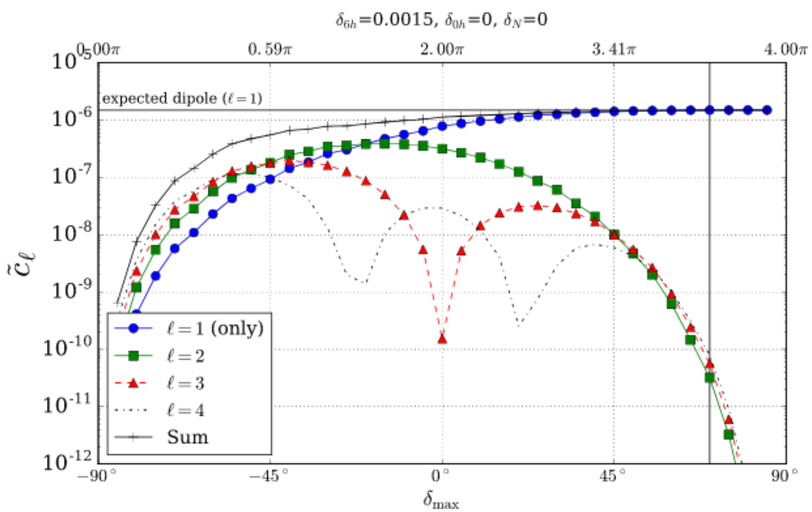

Figure 9. Angular power spectrum as a function of sky coverage for $\ell = \{1, 2, 3, 4\}$. The horizontal axis indicates the maximum decl. δ_{max}, keeping $\delta_{min} = -90°$ for a dipole injected horizontally in direction δ_{6h}. The partial coverage of sky produces an artificial quadrupole and octupole that decrease in power with greater celestial coverage.

https://iopscience.iop.org/article/10.3847/1538-4357/aaf5cc/pdf

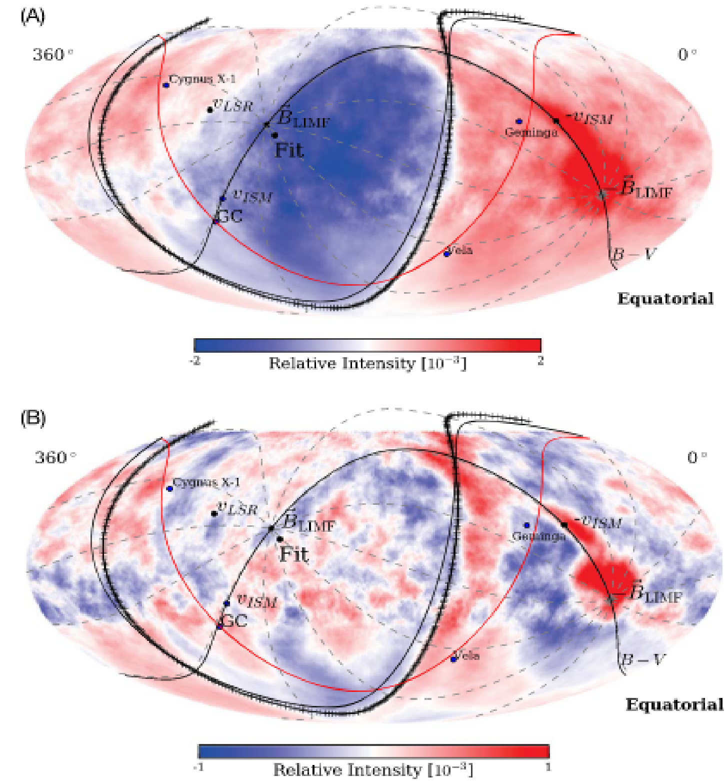

Figure 11. (A) Relative intensity of cosmic rays at 10 TeV median energy (Figures 4(A)) and (B) corresponding small-scale anisotropy (Figure 5(A)) in J2000 equatorial coordinates with color scale adjusted to emphasize features. The fit to the boundary between large-scale excess and deficit regions is shown as a black crossed curve. The magnetic equator from Zirnstein et al. (2016) is shown as a black curve, as is the plane containing the local interstellar medium magnetic field and velocity (B–V plane). The Galactic plane is shown as a red curve, and two nearby supernova remnants, Geminga and Vela, are shown for reference, as is Cygnus X-1, a black hole X-ray binary known to produce high-energy γ rays (Albert et al. 2007).

Cosmic Ray Anisotropy – All Sky

Table 1
Comparison of the IceCube and HAWC Data Sets

	IceCube		HAWC	
Latitude	90°S		19°N	
Detection method	Muons produced by CR		Air showers produced by CR and γ	
Field of view	$-90°/-16°$ (δ), $\sim$4 sr (same sky over 24 hr)		$-30°/68°$ (δ), $\sim$2 sr (8 sr observed/24 hr)	
Livetime	1742 days over a period of 1826 days		519 days over a period of 653 days	
Detector trigger rate	2.5 kHz		25 kHz	
	Quality cuts	Energy and quality cuts	Quality cuts	Energy and quality cuts
Median primary energy	20 TeV	10 TeV	2 TeV	10 TeV
Approx. angular resolution	2°–3°	2°–6°	0°.4–0°.8	0°.4–1°.0
Events	2.8×10^{11}	1.7×10^{11}	7.1×10^{10}	2.8×10^{10}

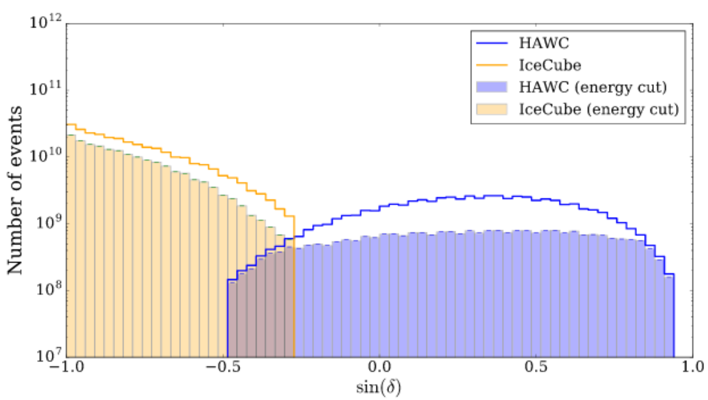

Figure 1. Distribution of events as a function of decl. for IceCube and HAWC. The figure shows the two data sets before and after applying energy and quality cuts. Restricting data sets to overlapping energy bins significantly reduces statistics for HAWC. The rates are dominated by events with energies near the threshold of each detector. By imposing an artificial cut on low energies in the HAWC data, the detector response flattens as it becomes less dependent on the zenith angle. The statistics in HAWC with 300 tanks before cuts are comparable to 1 year of IceCube with 86 strings.

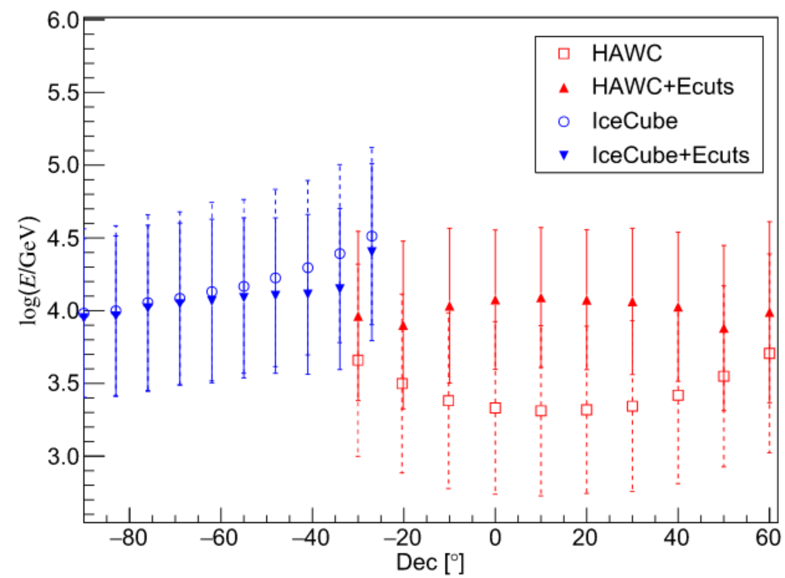

Figure 3. Median energy as a function of decl. for Monte Carlo simulations before and after applying energy cuts.

Cosmic Ray Anisotropy – All Sky

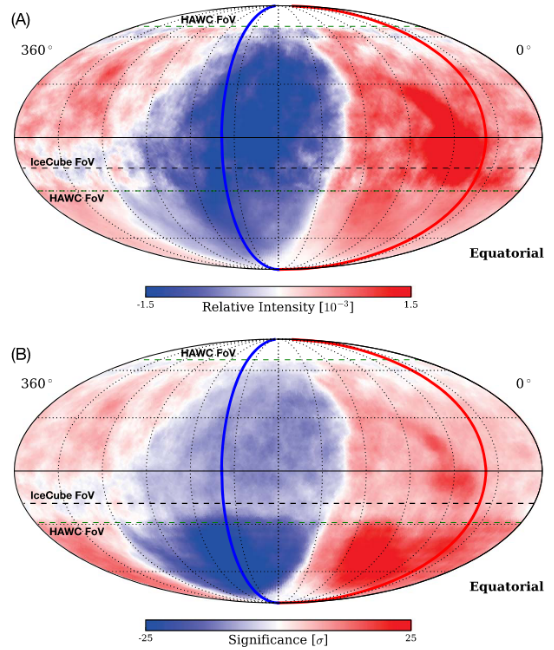

Figure 4. Mollweide projection sky maps of (A) relative intensity δI_a (Equation (2)) of cosmic rays at 10 TeV median energy and (B) corresponding signed statistical significance S_i (Equation (3)) of the deviation from the

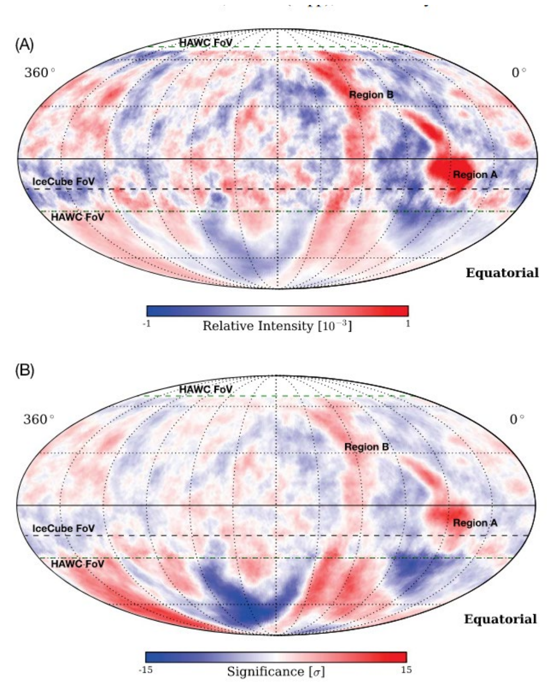

Figure 5. (A) Relative intensity δI_a (Equation (2)) after subtracting the multipole fit from the large-scale map and (B) corresponding signed statistical

Table 4
Magnetic Field Alignment

Source	R.A. [°]	Decl. [°]	$\Delta\psi$ [°]	δ_N [10^{-4}]
Funsten et al. (2013)	229.7 ± 1.9	23.3 ± 2.5	9.0	−5.03
Frisch et al. (2015)	237.9 ± 16	22.2 ± 16	12.2	−4.77
Zirnstein et al. (2016)	234.4 ± 0.7	16.3 ± 0.6	6.5	−3.42
Boundary Fit	229.2 ± 3.5	11.4 ± 3.0	⋯	−2.36
Dipole/Quadrupole	218.4 ± 0.3 (±2.6)	20.7 ± 0.3 (±2.6)	⋯	−4.41

Note. The last two rows correspond to measurements of the large-scale anisotropy from this study. The R.A. measurement in the last row is obtained from the dipole vector, and the decl. is obtained from the $\ell = 2$ quadrupole component. The second to last column corresponds to the angular distance $\Delta\psi$ between the boundary fit and the various LIMF estimates. The last column gives the corresponding vertical dipole component under the assumption that the dipole is oriented toward the given decl. Error in parentheses for dipole and quadruple correspond to systematic uncertainties.

Cosmic Ray Accelerators

nature › nature astronomy › letters › article

https://arxiv.org/abs/2103.06820

Letter | Published: 11 March 2021

HAWC observations of the acceleration of very-high-energy cosmic rays in the Cygnus Cocoon

Cosmic rays with energies up to a few PeV are known to be accelerated within the Milky Way. Traditionally, it has been presumed that supernova remnants were the main source of very-high-energy cosmic rays but theoretically it is difficult to get protons to PeV energies and observationally there simply is no evidence to support the remnants as sources of hadrons with energies above a few tens of TeV. One possible source of protons with those energies is the Galactic Center region. Here we report observations of 1-100 TeV gamma rays coming from the 'Cygnus Cocoon', which is a superbubble surrounding a region of OB2 massive star formation. These gamma rays are likely produced by 10-1000 TeV freshly accelerated CRs originating from the enclosed star forming region Cygnus OB2. Hitherto it was not known that such regions could accelerate particles to these energies. The measured flux is likely originated by hadronic interactions. The spectral shape and the emission profile of the Cocoon changes from GeV to TeV energies, which reveals the transport of cosmic particles and historical activity in the superbubble.

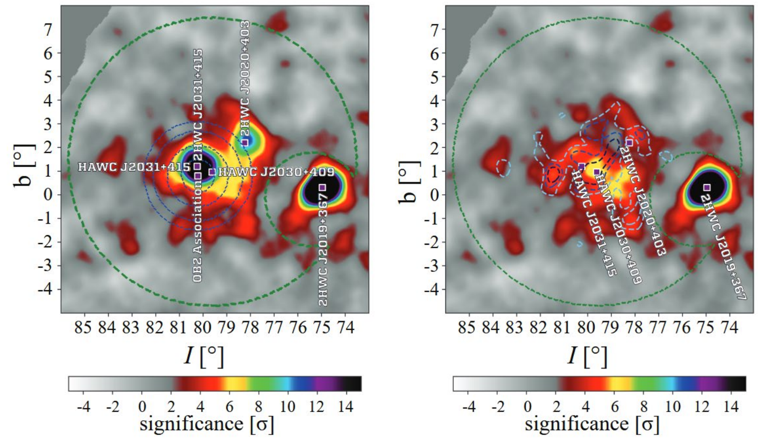

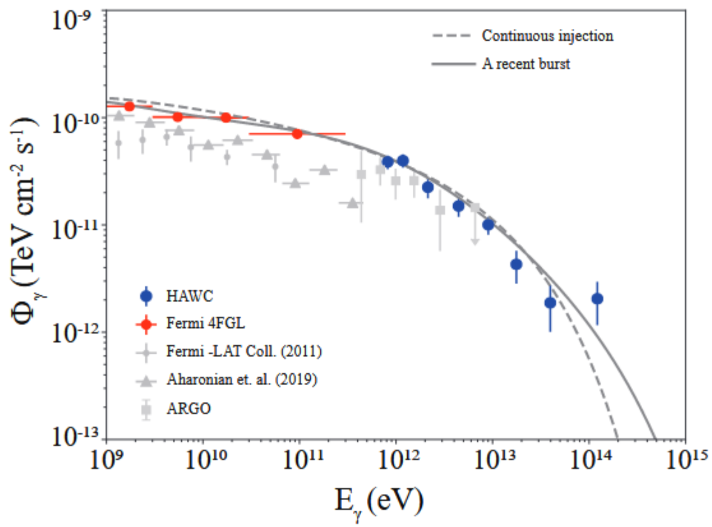

Energy Spectrum – hadronic modeling

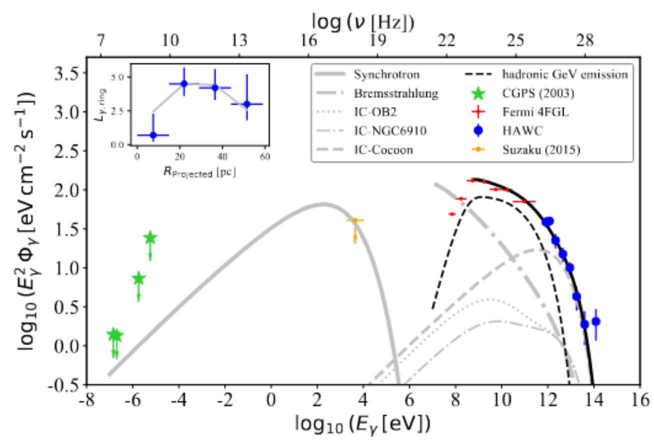

Energy Spectrum – leptonic modeling

Cosmic Ray Accelerators

HAWC J2227+610 and Its Association with G106.3+2.7, a New Potential Galactic PeVatron

Abstract

We present the detection of very-high-energy gamma-ray emission above 100 TeV from HAWC J2227+610 with the High-Altitude Water Cherenov Gamma-Ray Observatory (HAWC) observatory. Combining our observations with previously published results by the Very Energetic Radiation Imaging Telescope Array System (VERTIAS), we interpret the gamma-ray emission from HAWC J2227+610 as emission from protons with a lower limit in their cutoff energy of 800 TeV. The most likely source of the protons is the associated supernova remnant G106.3+2.7, making it a good candidate for a Galactic PeVatron. However, a purely leptonic origin of the observed emission cannot be excluded at this time.

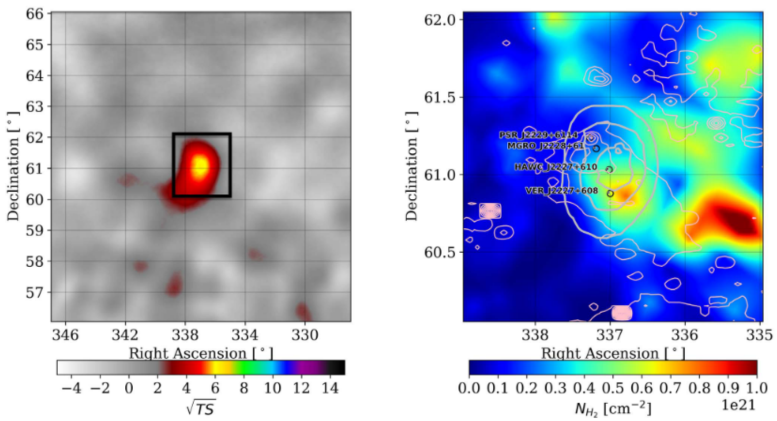

Figure 1. Left: HAWC significance map of the region, large-scale view. There are no other significant gamma-ray sources nearby that could affect the measurement. The black frame marks the size of the region shown on the right. Right: molecular hydrogen column density around HAWC J2227+610. See Appendix B for more details. The pulsar position as well as the centroids of the VERITAS and Milagro sources have been marked. The gray contours show the 1σ, 2σ, and 3σ confidence regions for the HAWC source position. The pink contours show the 1.4 GHz continuum brightness temperature from the Canadian Galactic Plane Survey (Taylor et al. 2003) in 50 logarithmically spaced steps from 1 to 100 K. Both maps have been smoothed and interpolated for display.

https://iopscience.iop.org/article/10.3847/2041-8213/ab96cc/pdf

- ❑ Galactic Gamma-Ray sources may be PeVatrons – sources of cosmic rays
- ❑ Spectrum of Gamma Rays may be of hadronic origin
- ❑ Multimessenger observations of neutrinos from these objects may be possible with future upgrades

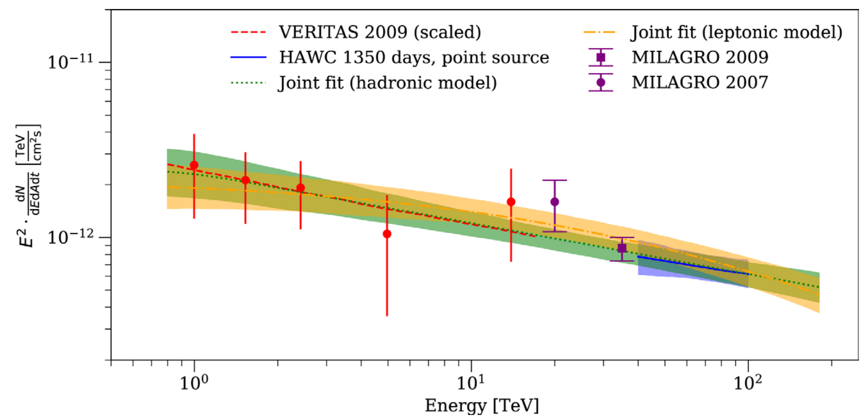

Even More Cosmic Ray-Related Studies with HAWC

- Constraining p-bar/p ratio using Moon shadow
  https://journals.aps.org/prd/pdf/10.1103/PhysRevD.97.102005
- Discovery of Gamma Rays from the Quiescent Sun with HAWC
  https://journals.aps.org/prl/pdf/10.1103/PhysRevLett.131.051201
- High-altitude characterization of the Hunga pressure wave with cosmic rays by the HAWC observatory https://www.sciencedirect.com/science/article/pii/S0273117723007858
- Characterization of the background for a neutrino search with the HAWC observatory https://doi.org/10.1016/j.astropartphys.2021.102670
- Probing the Sea of Cosmic Rays by Measuring Gamma-Ray Emission from Passive Giant Molecular Clouds with HAWC https://doi.org/10.3847/1538-4357/abfc47
- HAWC as a Ground-Based Space-Weather Observatory
  https://link.springer.com/article/10.1007/s11207-021-01827-z
- Interplanetary magnetic flux rope observed at ground level by HAWC
  https://iopscience.iop.org/article/10.3847/1538-4357/abc344

Summary and Future Outlook

- Many cosmic ray studies performed with conclusive results
- Analysis techniques still being improved, most notably the incorporation of machine learning techniques improving energy estimation.
- Several Articles in Development or under Collaboration Review
  - "A measurement of the intensity spectrum of cosmic rays from 10^{13} to 10^{15} eV using HAWC." – Update due to better energy resolution and smaller systematics. In collaboration review
  - "Cosmic Ray Composition dependent energy spectrum H,He and Heavy" – Analysis in progress
  - "Update on Cosmic Ray Anisotropies" – Analysis in progress using 8 years of data and improved techniques and control of systematics (Energy Spectrum Anisotropy? Mass separation?) – Analysis in progress
  - Solar physics studies –Magnetic Flux ropes, …. – Analysis in progress
  - Nearly Horizontal Muon Studies – Flux vs Depth in nearby volcanoes, Temperature Dependence of Horizontal Muon Flux – Analysis in progress

The HAWC Collaboration

USA:
Pennsylvania State University
University of Maryland
Los Alamos National Laboratory
University of Wisconsin
University of Utah
Univ. of California, Irvine
University of New Hampshire
University of New Mexico
Michigan Technological University
NASA/Goddard Space Flight Center
Georgia Institute of Technology
Colorado State University
Michigan State University
University of Rochester
University of California Santa Cruz

Europe:
Max Planck Institute KernPhysik Heidelberg
Krakow Nuclear Institute, Poland

Mexico:
Instituto Nacional de Astrofísica, Óptica y Electrónica (INAOE)
Universidad Nacional Autónoma de México (UNAM)
- Instituto de Física
- Instituto de Astronomía
- Instituto de Geofísica
- Instituto de Ciencias Nucleares

Universidad Politécnica de Pachuca
Benemérita Universidad Autónoma de Puebla
Universidad Autónoma de Chiapas
Universidad Autónoma del Estado de Hidalgo
Universidad de Guadalajara
Universidad Michoacana de San Nicolás de Hidalgo
Centro de Investigación y de Estudios Avanzados
Instituto Politécnico Nacional
Centro de Investigación en Computación - IPN

Central America:
University of Costa Rica

References

- https://journals.aps.org/prd/abstract/10.1103/PhysRevD.105.063021
- https://journals.aps.org/prd/abstract/10.1103/PhysRevD.105.063021
- https://doi.org/10.3847/1538-4357/aad90c
- https://iopscience.iop.org/article/10.3847/1538-4357/aaf5cc/pdf
- Measurement of the Crab Nebula Spectrum Past 100 TeV with HAWC https://iopscience.iop.org/article/10.3847/1538-4357/ab2f7d

Backup slides

EAS Reconstruction – Hit finding

TDC "hit"

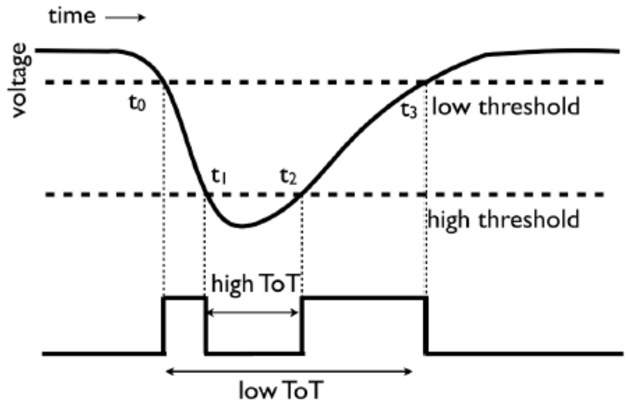

"Low TOT"

"t_0"

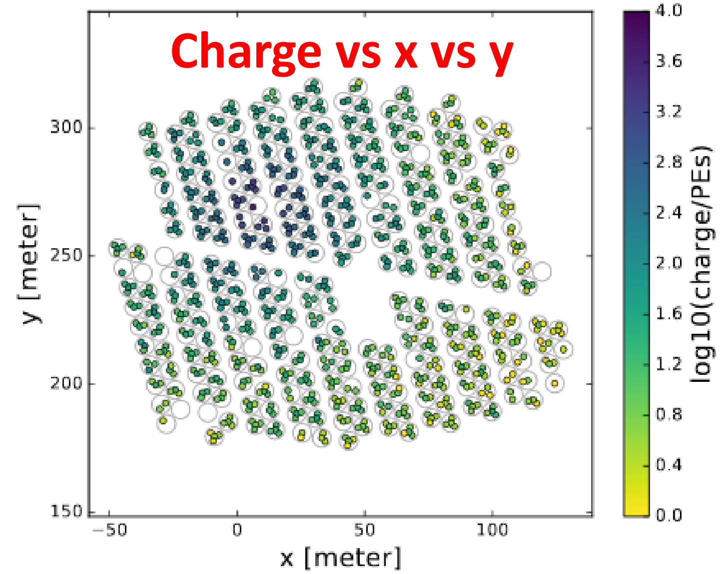

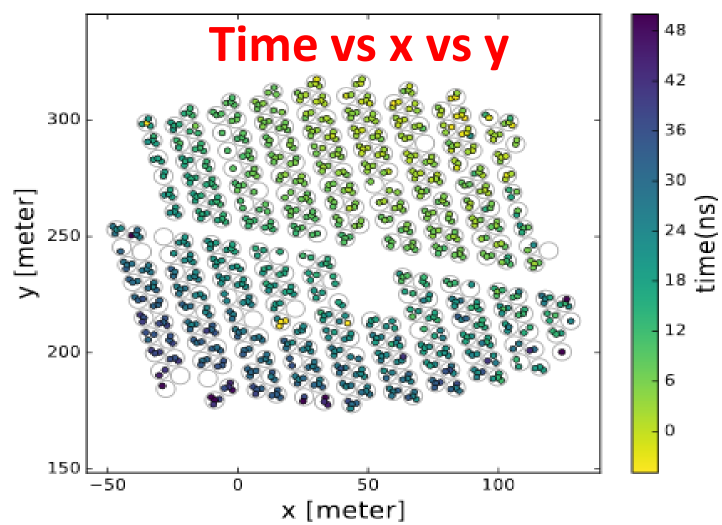

- Identify & remove noise hits.
- Reconstruct shower plane with good hits

Charge and Time vs position plots are from a high confidence gamma ray from the Crab Nebula

Observation of the Crab Nebula with the HAWC Gamma-Ray Observatory
HAWC Collaboration: A.U. Abeysekara et al., ApJ **843** (2017), 39.

EAS - Energy Reconstruction

Energy Estimator

Shower "size" bin $\mathcal{B}$ ($f_{hit}=N_{hit}/N_{tot}$)

Bin	N_{chan} Bin	E_{log} (GeV)	$\sigma_{E_{log}}$
1	39–59	2.5	0.46
2	60–69	2.6	0.47
3	70–90	2.7	0.44
4	91–147	2.9	0.40
5	148–231	3.0	0.35
6	232–349	3.2	0.32
7	350–495	3.5	0.28
8	496–655	3.7	0.24
9	656–789	3.8	0.21
10	790–1200	4.0	0.18
11	790–1200	4.2	0.18
12	790–1200	4.6	0.07
13	790–1200	5.1	0.13
14	790–1200	5.5	0.10

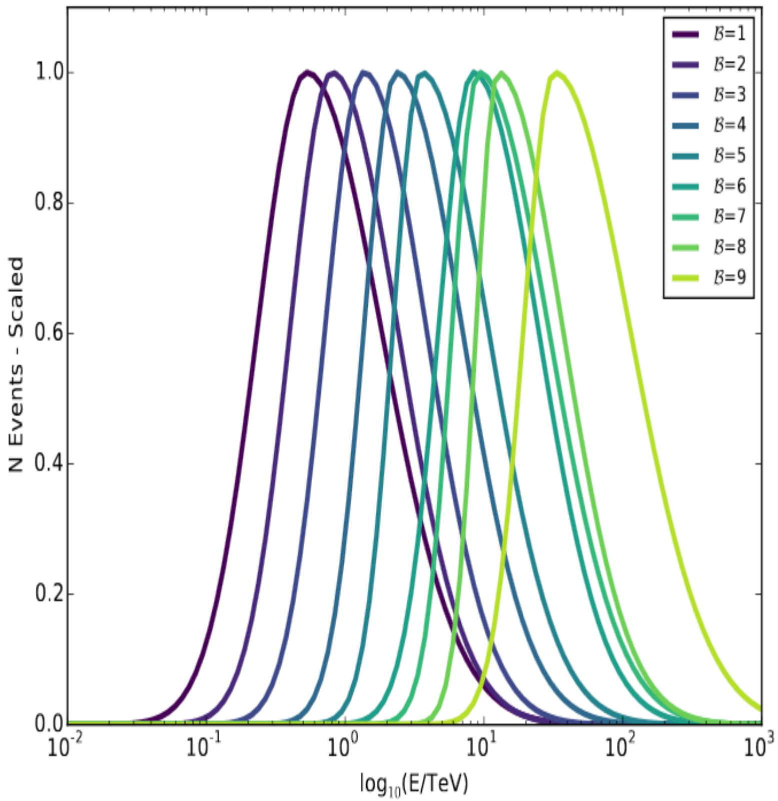

EAS - Energy Reconstruction

Energy Estimator

Neural Net Estimator

- Energy deposited in detector.
- Fraction of ground energy landing in detector.
- Fraction of primary energy reaching the ground.

http://adsabs.harvard.edu/abs/2017APS..APR.X4005M

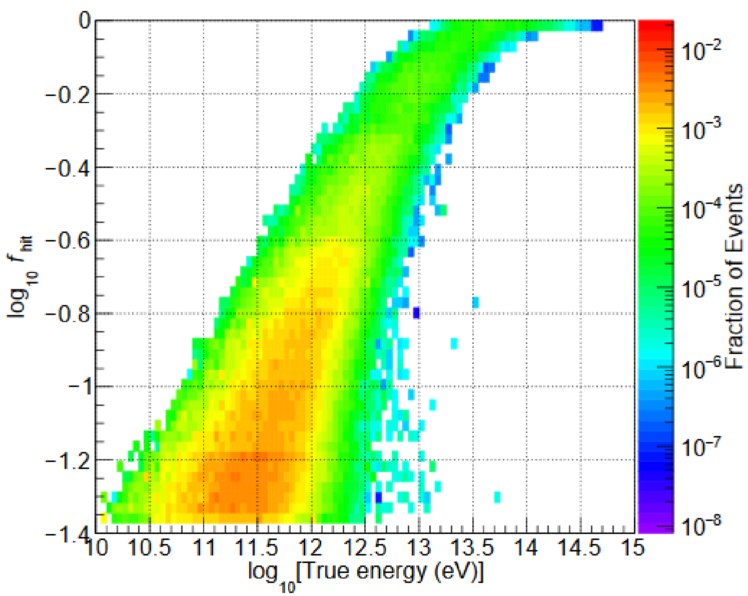

Fraction of PMTs hit

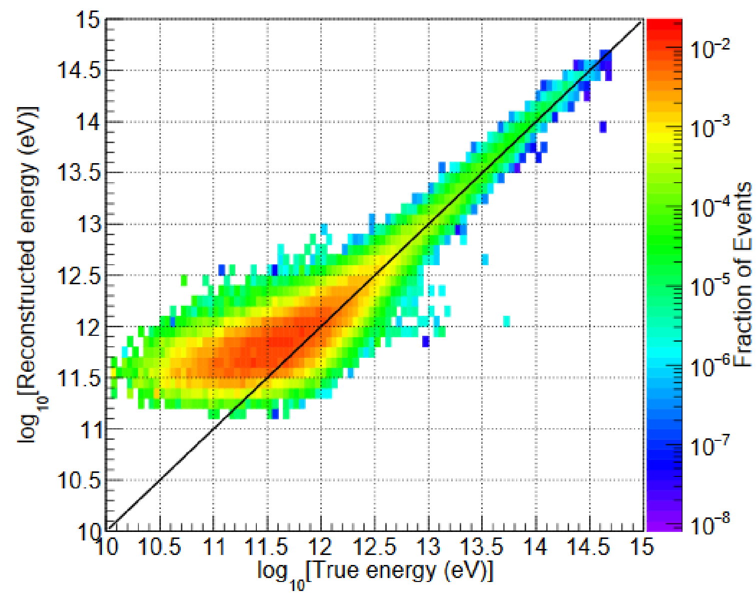

NN energy

EAS- Arrival Direction Resolution (Crab Measured)

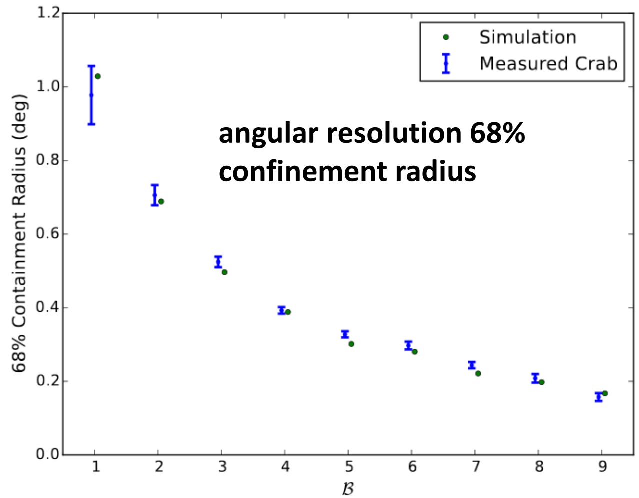

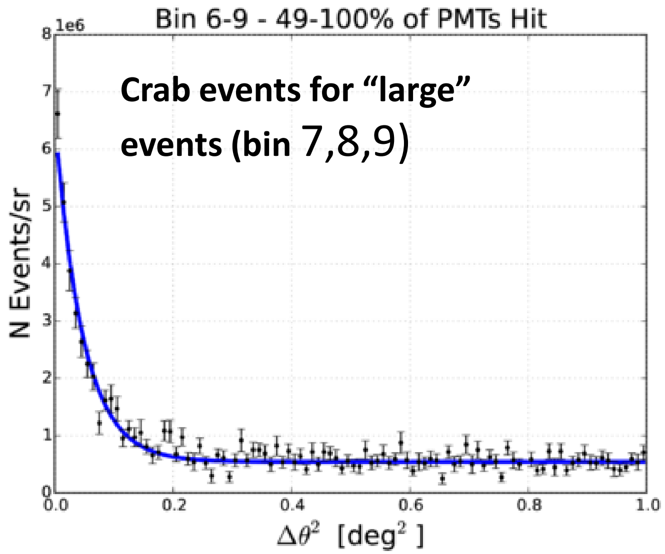

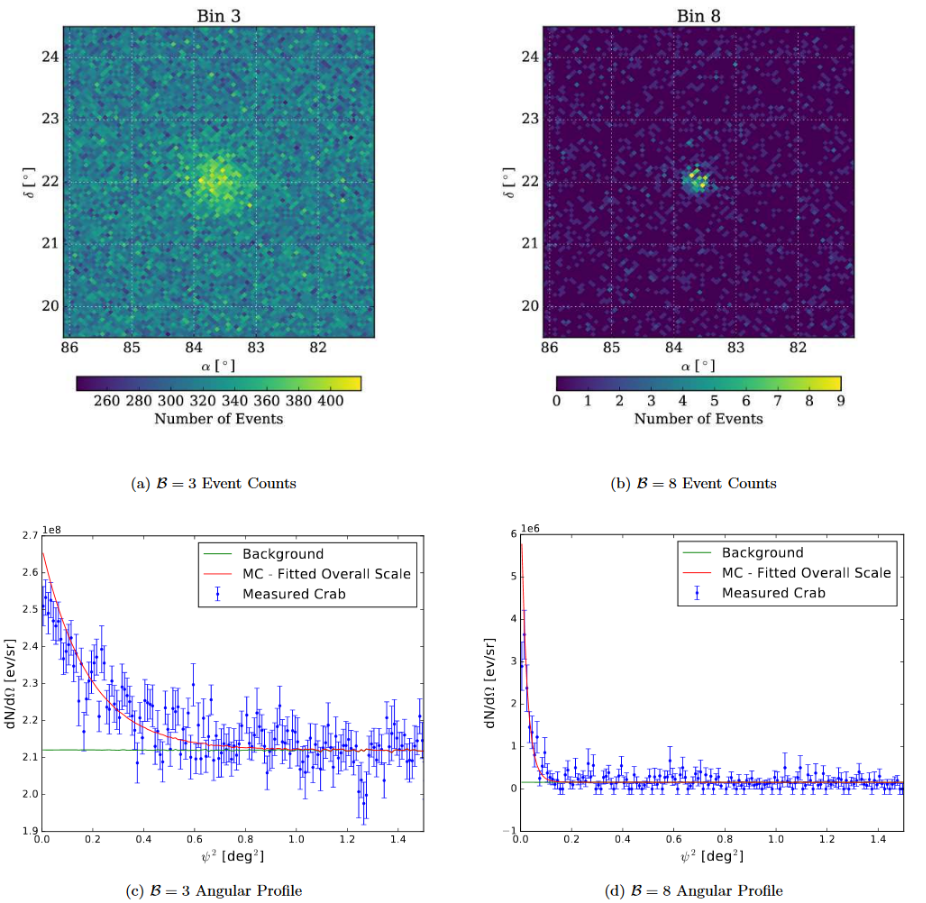

Figure 8. Maps of the sky around the Crab Nebula for events $\mathcal{B}$=3 (left) and $\mathcal{B}$=8 (right) after photon/hadron discrimination in equatorial coordinates. The top panels show the recorded number of events pixels on the sky much smaller than the HAWC angular resolution. The Crab is readily evident. The bottom panels show the number of recorded events per steradian (dN/dΩ) as a function of the distance from the Crab. At higher $\mathcal{B}$, the angular resolution and background rejection improve dramatically.

Galactic Results - Crab Observations & Spectrum

Crab Nebula provides a "bright" source of gamma rays that is "constant"…sometimes

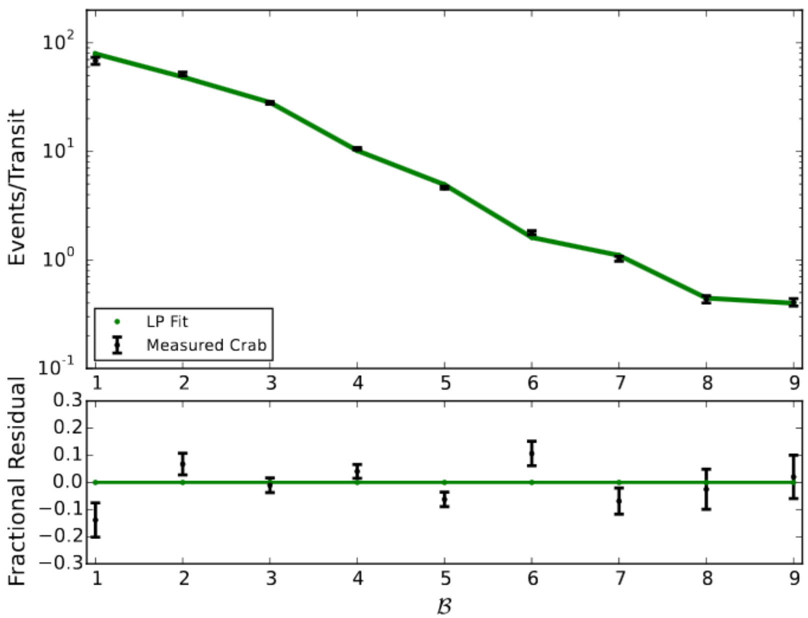

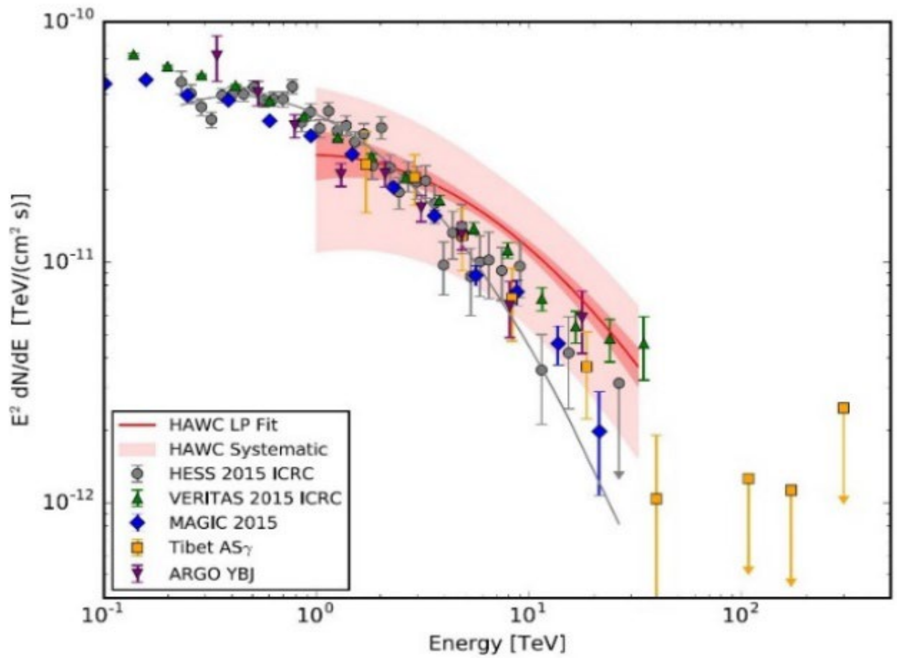

The spectrum of the Crab is fit to a function of the form $\phi(E) = \phi_0 (E/E_0)^{-\alpha-\beta \cdot \ln(E/E_0)}$. The data is well fitted with values of α = 2.63 ± 0.03, β = 0.15 ± 0.03, and $\log_{10}(\phi_0 \text{ cm}^2 \text{ s TeV}) = -12.60 \pm 0.02$ when E_0 is fixed at 7 TeV and the fit applies between 1 and 37 TeV. Study of the systematic errors in this HAWC measurement is discussed and estimated to be ±50% in the photon flux between 1 and 37 TeV. Confirmation of the Crab flux serves to establish the HAWC instrument's sensitivity for surveys of the sky.

ApJ **843** (2017), 39.